Chapter 1
Tribology of Thermal-Sprayed Coatings

R.J.K. Wood and Manish Roy

1.1 Introduction

Thermal spraying refers to a group of processes that apply consumable powders or wires in the form of finely divided molten and semi-molten droplets to produce coatings. Thermal spraying dates back to 1911 when Dr. Schoop was successful in atomising molten metal by high pressure gas and propelled them on to a surface. In 1912 he produced a device to spray metal wires and this process is known as flame spraying. Subsequently he introduced new technique for thermal spraying by using electricity to melt feedstock materials. This method in present times is referred as arc spraying. The idea of using powder for the flame spraying process was developed for the first time by F. Schori in 1930.

The above-mentioned processes can use only low melting metallic powders. Slowly demand for powders with high melting temperature and oxidation resistance aroused. The demand for spraying cermet or ceramic powder saw development of detonation spraying in 1955 and atmospheric plasma spraying in 1960. This was followed by development of vacuum plasma spraying (VPS) and low-pressure plasma spraying (LPPS) in late 1970 and 1980. The major development of thermal spraying occurred in 1980 when a novel technique for spraying powder employing high oxygen, known as high velocity oxy-fuel (HVOF) technique was introduced. The year 1990 experienced the development of most important technology cold spraying. This process has the ability to produce unique coating that is not possible by other coating method.

R.J.K. Wood (✉)
National Center for Advanced Tribology, University of Southampton, Southampton, UK
e-mail: rjw3@soton.ac.uk

M. Roy
Defence Metallurgical Research Laboratory, Kanchanbagh, Hyderabad 500058, Andhra Pradesh, India

M. Roy (ed.), *Surface Engineering for Enhanced Performance against Wear*,
DOI 10.1007/978-3-7091-0101-8_1,

Important advantages of thermal spraying process are ease of processing, ease of selection of substrate and no heating of the substrate. Several extensive reviews on this process can be found in [1–5]. This chapter tries to give recent development and the data base of thermal-sprayed coatings for tribological applications in various industrial sectors.

1.2 Process Classifications and Fundamentals

Thermal spray processes can be classified into three different categories. The first group uses combustion as heat sources. The second variety uses electrical energy either in the form of plasma or as an arc. The third variety is cold spraying. This is a process by itself. Low velocity combustion also known as flame spraying (FS) and high velocity combustion are two different combustion-spraying methods. The maximum temperature attained in both cases are, in general, comparable as similar fuel gases such as propylene, propane, acetylene or hydrogen or liquid fuel such as kerosene, etc., are commonly used. In all cases, oxygen is used as oxidant. In case of high velocity process, it is called high velocity oxy-fuel (HVOF) as against flame spraying for low velocity combustion; sometimes atmospheric air is used as oxidant and the process is termed as high velocity air fuel (HVAF). In case of low velocity technique, the dwell time of particles in the gas is more than the high velocity technique and consequently oxidation and degradation of the particles are more. This results in formation of coating with higher porosity and lower or moderate (around 50–75 MPa) bond strength. However, flame spraying process permits higher deposition rate as course powder or wire is used. This process is portable, less noisy and economical.

In case of high velocity technique, the dwell time of the powders is much less of the order of microsecond resulting in less oxidation and degradation of coating powders. This permits use of fine powders, which can be propelled to the substrate with high velocity. Consequently, a coating with minimum porosities less than 0.5 % and good bond strength is possible. Further deposition with high velocity permits spraying powders with higher melting point and thus widening the range of application to include high temperature coatings, thermal- and shock-resistant coatings. Deposition of coating at high velocity using wire permits continuous deposition. However, there are far less varieties of wire than powders. Most of these HVOF processes are continuous combustion process. In contrast, detonation gun process which uses spark discharge to propel powder is a repeated cyclic process. However, D-gun process is extremely noisy.

HVOF processes can broadly be divided under two different heads depending on their burners. These are throat combustion burners and chamber combustion burners. In throat combustion process, powder is introduced axially. Detonation gun, as shown schematically in Fig. 1.1, can be considered as an example of throat combustion process. Many system based on throat combustion process suffered from the disadvantage of short barrel, lower velocity and reduced particle heating.

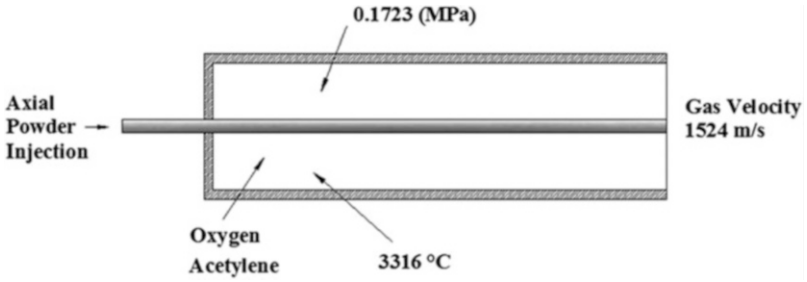

Fig. 1.1 Schematic representation of detonation-sprayed coatings

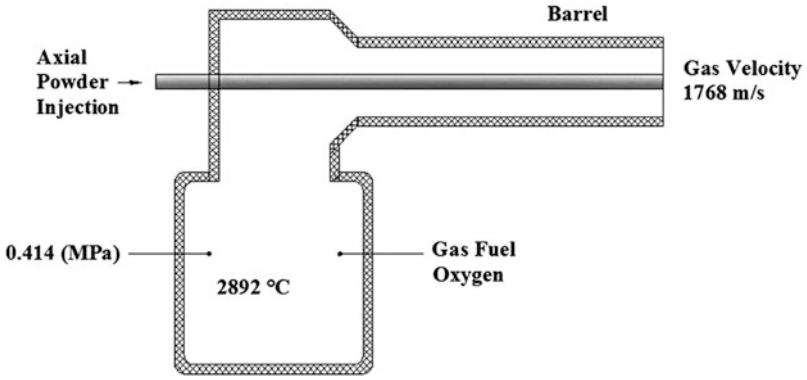

Fig. 1.2 Schematic diagram of jet kote process

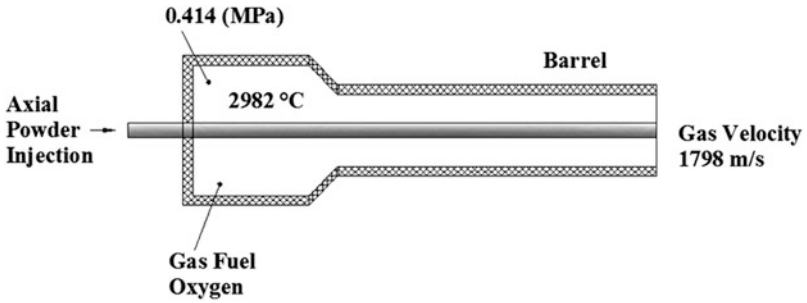

Fig. 1.3 Schematic diagram of top gun or continuous detonation process

In chamber combustion process, powder is fed both radially or axially. Jet Kote shown in Fig. 1.2 pertains to an axially injected water cooled process having combustion chamber at right angle. In contrast, Top gun or continuous detonation gun presented schematically in Fig. 1.3 is an example of throat combustion process with coaxial combustion chamber for axial injection. Finally JP 5000 represents a

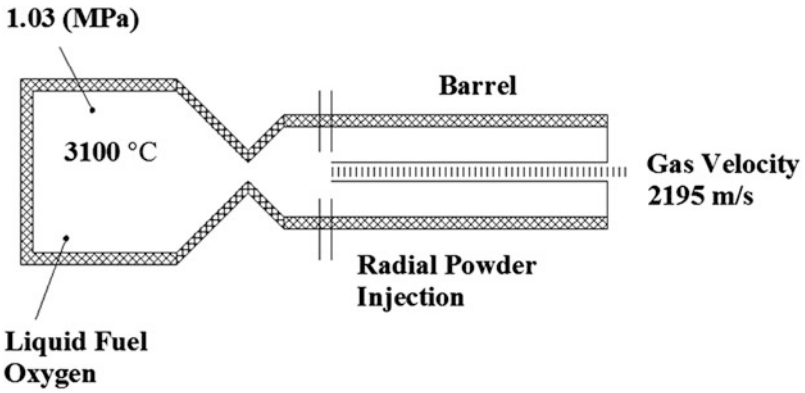

Fig. 1.4 Schematic of JP 5000 gun

double chamber, radial injection chamber combustion process which uses liquid fuel. JP 5000 is shown schematically in Fig. 1.4.

Plasma and electric arc are two different processes of thermal spraying techniques driven by electrical energy. In the wire arc spraying process, high temperature generated in the arc is used to melt feedstock materials. In contrast, in plasma spraying process, electrical energy is utilised to ionise gas medium. Plasma spraying is extremely versatile as it can be used to spray metallic, cermet as well as ceramic powders. A large variety of powder with coarser dimension can be used. This equipment is quite sophisticated, emits ultraviolet rays and needs skilled operator. There are three different types of plasma spraying processes, namely, atmospheric plasma spraying, (APS), low pressure plasma spraying (LPPS) and vacuum plasma spraying (VPS). Choice of the process depends on the powders to be sprayed and their applications.

1.3 Powder Production Methods

Depending on the nature of powder required, various production methods are adopted. In general, atomisation is one of the most popular methods of production of powders of metals and alloys. In atomisation method, molten metal or alloy is poured in a heated funnel connected to a nozzle where it is finely dispersed either by water or by gas. Sometimes dispersion is carried out by centrifugal method which is far more energy efficient than gas or water atomisation methods. Low melting solder powders are produced by spinning disc atomisation techniques which has yield as high as 70 %. Higher melting point powders such as zinc (for batteries), aluminium (for chemicals), etc., are produced by spinning cup atomisation technique with very high yield, even higher than 70 % yield. Highly corrosive powders such as Ti powders are produced by rotating electrode method. This method

provides powder with exact standard of cleanliness and smaller range of size distribution than gas atomisation method. Ultrasonic gas atomisation or vibrational ultrasonic atomisation also finds applications when perfectly spherical powder with narrower range of composition is required. Roller atomisation, vibrating electrode atomisation and melt drop atomisation are other atomisation techniques which are still in experimental stages. Powders produced by atomisation technique are spherical. The composition and the phases of the powders depend on the methods of atomisation or dispersion.

Most of the ceramic powders are produced by fusion and crushing methods. In this method the required material is melted in a furnace and then solidified as an ingot. The ingot is subsequently crushed in industrial crushing mills. Powders manufactured in this method are dense, blocky and are of irregular shapes.

Metal powders are also produced by chemical or electrolytic method. These methods allow wide variety of powder production with close control of composition, shape and size of powders. Oxide reduction for powder production is a well-established commercial process. Powders of metals with high melting point such as tungsten and molybdenum can be produced by this method for economic reason. Further, these powders are stabilised against tarnishing.

Production of metal powders from hydrometallurgical processing is based on leaching an ore concentrate followed by precipitation of metal from the leach solution by electrolysis, cementation or by chemical reduction. It is possible to produce a large variety of powders with regard to size, shape, density and specific surface area employing this process with additives or control of particle growth, particle nucleation and particle agglomeration. By using co-precipitation or successive precipitation, it is possible to produce powders of various alloys and composites.

Thermal decomposition is another important chemical method for production of metal powders. Generally this method produces highly pure fine powders. Among other chemical powder production method, precipitation from salt solution, precipitation from gas, hydride decomposition and thermal reactions are worth mentioning.

It is possible to produce a large variety of metal powders by electro deposition. By direct electro deposition, loosely adhering powdery and spongy deposit can be obtained and these deposits can be disintegrated mechanically in fine powders. Dense, smooth and brittle layers of refined metal can be deposited and crushed into fine powders. Metals with high electrolytic polarisation can form highly brittle coherent deposit by brittle cathode process. This deposit can subsequently be granulated into fine powders.

Spray drying is a versatile method, which allows production of any kind of agglomerated powders using an organic binder phase. In this method, a mixture of organic binder, water and the materials to be agglomerated is sprayed in a chamber where hot dry gases are flowing. The water in the mixture evaporates and the organic binder covers the material particles, producing agglomerated powder. Powders produced by this method are porous and sometimes subjected to densification.

1.4 Types of Thermal Spray Coatings

Thermal spray coatings can be of different types. Many coatings are deposited as pure metals such as molybdenum, nickel, copper, tungsten, etc. Pure metals are deposited for both tribological and corrosion resistance applications. Various types of stainless steel, Hastalloys, Monels, etc., constitute alloy coatings. These coatings find applications primarily as corrosion resistance layer. WC–Co and Cr_3C_2–NiCr are most popular variety of cermet powders used in general for wear resistance applications. Finally, a large variety of ceramic powders such as ZrO_2, Al_2O_3, yttria-stabilized zirconia, etc., are employed for high temperature applications. Chemical inertness, excellent sealing properties due to high density and low porosity and outstanding friction characteristics have made polymer a viable protective coating. The variety of polyethylene, polyamide, poly-ether ether ketone, poly methylmethacrylate and other thermoplastic are sprayed successfully and found several engineering applications. Low friction materials dispersed in soft matrix are often termed abradable coatings. These coatings are used for clearance control between two moving parts. (Al–Si)–graphite, Ni–Graphite, (Al–Si) polyester are some examples of abradable coating. Self-fluxing powders constitute another variety of coatings. These are the powders that are designed to remelt on spraying. These powders contain elements like boron and silicon which reacts with oxygen and form a slag over the molten coating producing an oxygen-free metallic coating containing finely dispersed boride and nitride particles. These coatings are excellent for high temperature tribological applications.

1.5 Properties of Thermal Spray Coatings

The properties of thermal spray coatings are governed by chemical composition, porosities and oxide content of the coatings. In thermal spray coatings, many properties are determined by splat morphology, interfacial strength of splat–splat interface and splat–substrate interface.

1.5.1 Microstructural Features

WC–17 % Co with a range of particle size '08–64 μm' has been characterised. Typical SEM images of commercial spherical WC–17 % Co powders, spherical Cr_3C_2–25(Ni20Cr) powder, angular WC–12 % Co powder and spherical WC-12% powder are shown in Fig. 1.5 [6, 7]. All granulated powders are of spherical shapes with presence of comparatively large initial porosities. Presence of surface oxide on the spray granules were detected by SEM analysis. There are many applications where angular powders with different sizes and shapes are used. Angular powders are

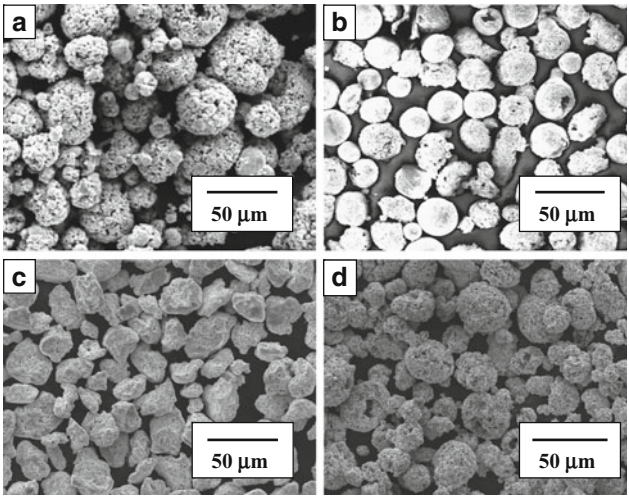

Fig. 1.5 SEM images of various powders. (**a**) Spherical WC–17 % Co powders, (**b**) spherical Cr_3C_2–25(Ni20Cr) powder, (**c**) angular WC–12 % Co powder and (**d**) spherical WC–12 % Co powder

easy to produce and if they are not sufficiently fine, resultant coatings have porosities. Very fine powders are difficult to feed at constant rate and sometimes they are responsible for high degree of oxidation or undesirable phase transformation.

The low magnification images of the sectioned surfaces of HVOF-sprayed Cr_3C_2–25(Ni20Cr) coating, detonation-sprayed WC–12 % Co coating and plasma-sprayed WC–12 % Co coating are shown in Fig. 1.6. The coatings exhibit reasonably good interface with the substrate as evident from the figure. The thickness of the coatings is around 200–300 µm. No cracks can be seen on the sectioned surfaces of the coatings. The coating is built by depositing lenticular splat one after the other. This type of stratified structure is common in HVOF spraying [8].

The high magnification SEM image of the detonation-sprayed WC–12 % Co coating on MS is illustrated in Fig. 1.7. In detonation-sprayed coating, there are evidences of insufficient melting. Splats of lenticular shapes are deposited one after the other. Figure 1.7 represents one of the cross-sectional micro-structure of the WC–17 % Co coating as observed in the plasma spray process (Fig. 1.7b) and HVOF process (Fig. 1.7c). The porosities on WC–17 % Co-coated surface as determined by image analysis were observed to be less than 0.5 %. The related percentage of unmelted particle was less than 0.2 % with exception to WC particles which are difficult to melt. WC is one of the hardest carbides with melting point as around 3,043 K. However the hot flattening behaviour of WC is significant in plasma spray process compared to that behaviour in HVOF process. This phenomenon leads to production of a dense and adherent coating by the plasma process. In such a process, the as-sprayed surface roughness (R_a) was about 1.5–2.1 µm.

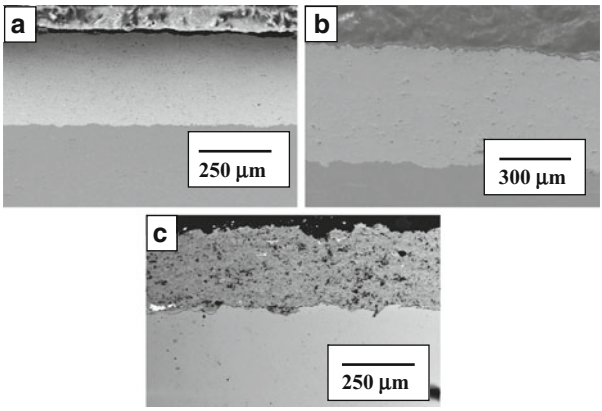

Fig. 1.6 The low magnification images of the sectioned surfaces of (**a**) HVOF-sprayed Cr_3C_2–25 (Ni20Cr) coating, (**b**) detonation-sprayed WC–12 % Co coatings and (**c**) plasma-sprayed WC–12 % Co coating

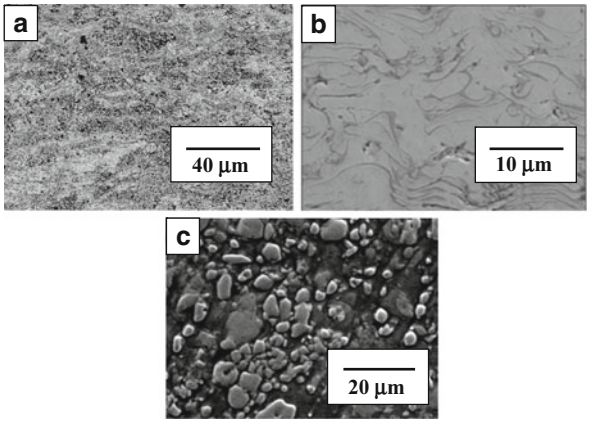

Fig. 1.7 The high magnification back-scattered images of the sectioned portion of (**a**) detonation-sprayed WC-12 % coating, (**b**) plasma-sprayed WC–12 % Co coating and (**c**) SEM image of HVOF-sprayed WC–17 % Co coating

The high magnification back-scattered images of the sectioned portion of detonation-sprayed WC-12 % coating and HVOF-sprayed Cr_3C_2–25(Ni20Cr) coating are given in Fig. 1.8. Pores (black areas) and oxides (circular black areas) are evident in coating. Image analysis of HVOF-sprayed Cr_3C_2–25(Ni20Cr) coating indicates 1.5 porosity and 0.75 % oxides in the coatings respectively. Examination of the coated microstructure also reveals the presence of three different types of zones. The first zone appears dark. The EDS spectrum from the dark area indicates that this area contains primarily Cr and C indicating orthorhombic Cr_3C_2 phase. The second zone is of grey colour. The EDS spectrum of this area reveals that this area contains all the three important elements, Ni, Cr and C. Quantitative analysis indicates this zone contains both Cr_3C_2 and NiCr. The third zone is white and the EDS spectrum pertaining to this zone reveals NiCr as the important phase. The quantitative analysis of these zones is given in Table 1.1.

The transmission electron micrograph from an arbitrary zone of the Cr_3C_2–25 (Ni20Cr) coating is illustrated in Fig. 1.9a along with the electron diffraction pattern and EDS spectrum [9]. Very fine grain size of the order of 40–80 nm is

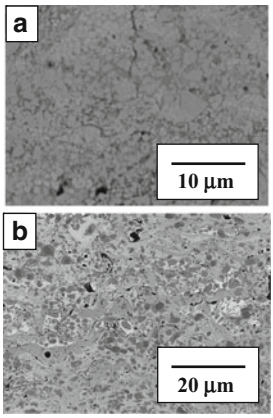

Fig. 1.8 The high magnification back-scattered images of the sectioned portion of detonation-sprayed WC-12 % coating and HVOF-sprayed Cr_3C_2–25 (Ni20Cr) coating

Table 1.1 The composition of various elements as measured by EDAX

	Elements		
	C	Cr	Ni
Dark zone			
Wt%	16.05	83.04	0.91
At%	45.40	54.07	0.53
Grey zone			
Wt%	13.31	65.86	20.83
At%	40.68	46.30	13.03
White zone			
Wt%	12.72	58.66	28.62
At%	39.67	42.08	18.25

evident. The selected area diffraction (SAD) pattern also suggests fine grains. The EDS spectrum and the indexed diffraction pattern confirm the fact that the micrograph belongs to the dark zone containing Cr_3C_2 phase. There is some tendency for amorphisation as can be noted from the SAD pattern. This is consistent with the observation from X-ray diffraction pattern. The bright field transmission electron micrographs along with electron diffraction pattern and EDS spectrum from another area are presented in Fig. 1.9b. The indexed electron diffraction pattern and EDS spectrum confirm a mixture of FCC NiCr and orthorhombic Cr_3C_2 phases. Representative TEM bright field images, corresponding electron diffraction pattern of another area, are given in Fig. 1.9c. The grains in this area are very fine, around 25 nm of size. The crystallinity of the area is evident. Based on Fig. 1.9c, it can be concluded that the area contains primarily FCC NiCr structure. This observation is consistent with that noted by He and Lavernia [10], who found crystalline matrix of NiCr for Cr_3C_2–NiCr coating. In contrast, Guilemany and Calero [11] observed amorphous matrix phase in HVOF-sprayed conventional Cr_3C_2–NiCr coating. There are certain areas in the grey zone, which shows presence of an amorphous zone along with nanocrystalline region. This region is possibly the one which was melted during spraying. A rapid solidification is responsible for this amorphisation.

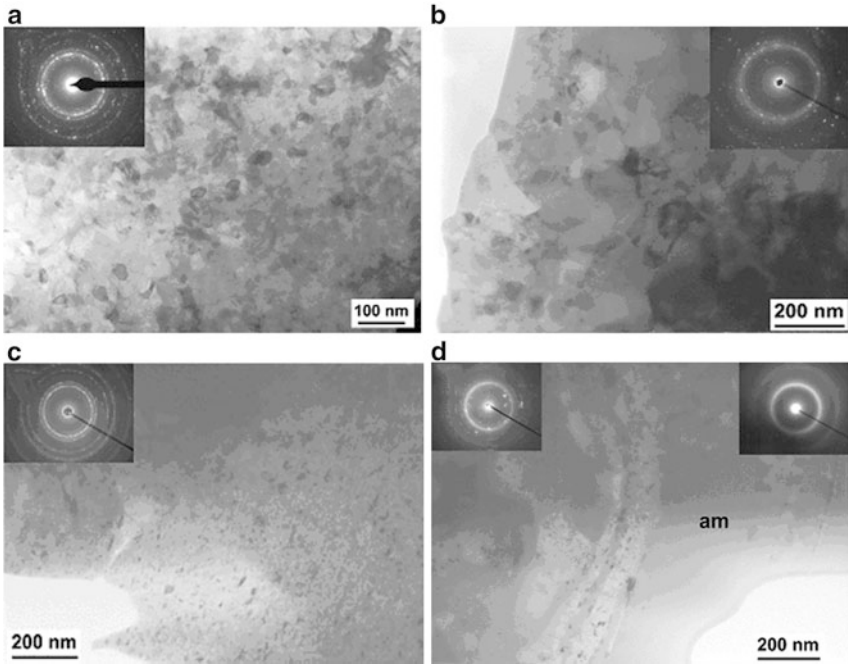

Fig. 1.9 Transmission electron microscopy image of Cr_3C_2–25(Ni20Cr) coating from an (**a**) area containing Cr_3C_2 phase, (**b**) area containing a mixture of FCC NiCr and orthorhombic Cr_3C_2 phases, (**c**) area containing primarily FCC NiCr structure and (**d**) area containing an amorphous zone

A typical TEM micrograph of this region is shown in Fig. 1.9d. A transition zone separates the purely amorphous area from an area containing a mixture of small crystals and remaining amorphous phase. Thus the coating obtained contains three different zones containing different proportion of orthorhombic Cr_3C_2 and FCC NiCr phases.

XRD pattern of WC–12 % Co powder, detonation-sprayed WC–12 % Co coating, WC–17 % Co powder and detonation-sprayed WC–17 % Co coating is shown in Fig. 1.10. Powders in both composition exhibit WC and Co phases. However, on spraying pure Co ceases to exist. Detonation spraying has resulted in partial amorphisation. While the powder contains primarily WC and Co, the coating contains W_2C and Co_6W_6C in addition to WC and phases. Small amount of amorphous Co can be seen in detonation-sprayed WC–17 % Co coating. Comparison of detonation-sprayed coatings and plasma-sprayed coating can be seen in Fig. 1.11 for WC–12 % Co coating and WC–17 % Co coating. In plasma-sprayed coating, unreacted Co can be seen. Further extent of decarburisation resulting in formation of W_2C phase is more in plasma-sprayed coating as compared to detonation-sprayed coatings.

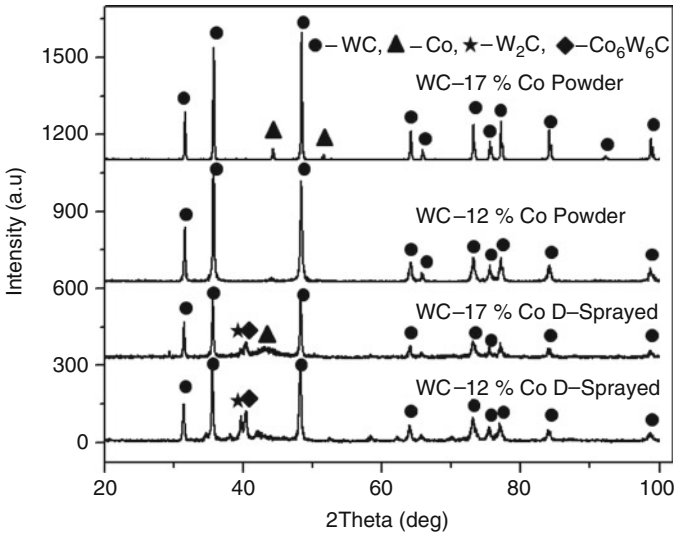

Fig. 1.10 XRD pattern of WC–12 % Co powder and detonation-sprayed coating and WC–17 % Co powder and detonation-sprayed coating

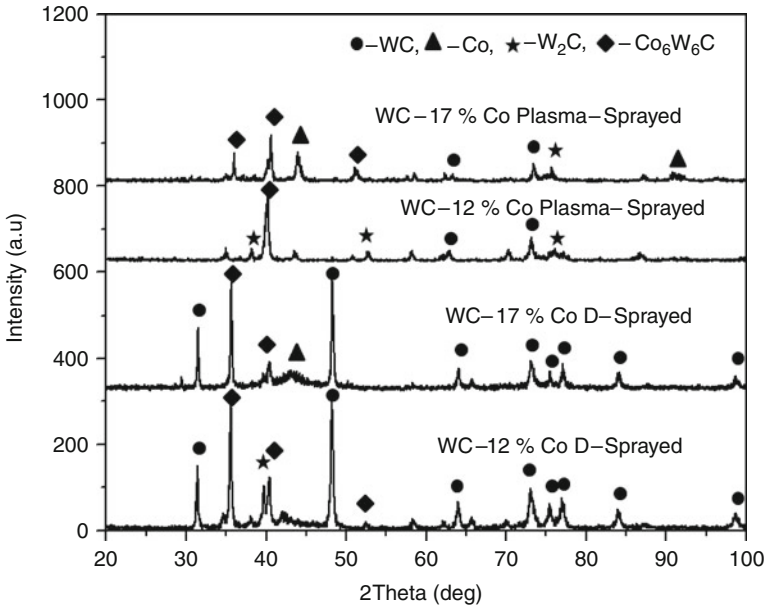

Fig. 1.11 XRD pattern of WC–12 % Co plasma-sprayed and detonation-sprayed coating and WC–17 % Co plasma-sprayed and detonation-sprayed coating

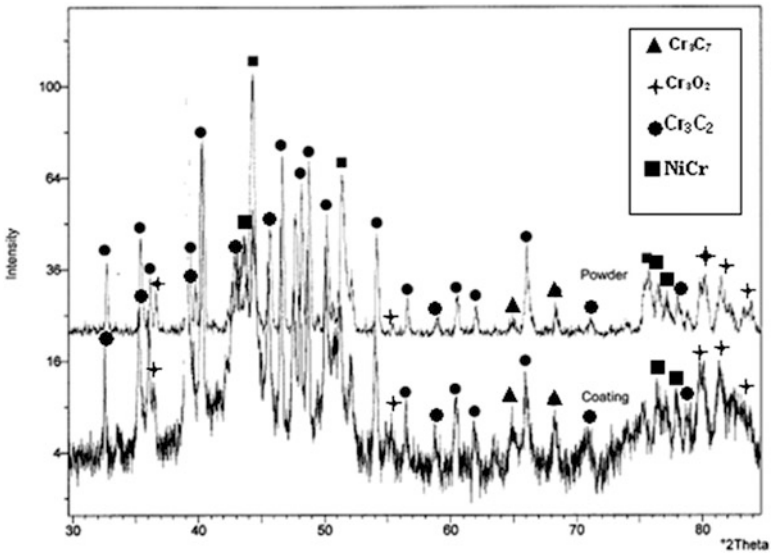

Fig. 1.12 XRD pattern of Cr_3C_2–25(Ni20Cr) powder and coating obtained by JP 5000 gun

The XRD pattern of the Cr_3C_2–25(Ni20Cr) powder and coating is shown in Fig. 1.12. Most important point to be noticed is that, there is no change of phases present in the powder. This is contrary to what is commonly observed for thermal-sprayed WC–Co coatings [12]. Interestingly, Mohanty et al. [13] observed a transformation of Cr_3C_2 phases to $Cr_{23}C_6$ phases while spraying Cr_3C_2–NiCr powder with conventional grain size by Jet Kote technique. Such dissociation of Cr_3C_2 phases is not noted in the present study even in the case of nanocrystalline grains. One possible reason for this phenomenon is that the residence time of the particles in the flame is much less for the spraying system with liquid fuel. Presence of Cr_3O_2 and Cr_3C_7 can be traced in the powder and in the coated surface. There is significant amount of amorphisation of the powder as a result of spraying.

1.5.2 Mechanical Properties

Most important mechanical property of thermal spray coatings is hardness. Mostly Knoop indenter is used to measure the hardness of thermal-sprayed coatings although Vickers indenter is used for measuring both hardness and indentation toughness. Details of Knoop indentation testing is given by Marshall et al. [14] and Leigh et al. [15]. Hardness using Knoop indenter can be given by

$$\mathrm{KHN} = 14,229\frac{P}{a^2} \tag{1.1}$$

where KHN is Knoop hardness number expressed in kg/mm^2, P is the applied load in gf and a is the length of the major diagonal of the indenter in μm. Elastic modulus can be determined using Knoop indenter following the equation given below:

$$\frac{b}{a} \approx \frac{b}{a'} = \frac{b'}{a'} - \frac{\alpha \mathrm{KHN}}{E} \tag{1.2}$$

where b is the minor diagonal of the indentation, a', b' are the major and minor diagonals of the ideal Knoop indentation, α is a constant and generally assumed to be 0.45 and E is the elastic modulus having same dimension as that of KHN. In general, b'/a' is equal to 0.14.

The hardness values so obtained follow mostly Normal, Lognormal and Weibull distributions [16]. However, Weibull distribution appears to be most suitable for thermal-sprayed coatings as properties distributions are highly screwed and broadly distributed [17]. The Weibull distribution in two parameter form may be given as

$$F(x) = 1 - \mathrm{e}^{-(x/x_o)^m} \tag{1.3}$$

where $F(x)$ is the cumulative density function of probability, x_o is scale parameter below which 63.2 % of the data lie and m is the Weibull modulus.

Indentation toughness of thermal-sprayed coatings is evaluated by using Vicker's indentor. The indentation can be carried out on the traverse section of the coating in the mid-plane region. The indentor should be loaded so that one of the horizontal diagonals is parallel to the coating substrate interface. The diagonals of the indentation ($2a$) and lengths of the cracks (l) at the corners of the indentation are measured and used to estimate characteristics crack length ($c = l + a$) and fracture toughness (K_i). For median/radial cracks ($c/a \geq 2.5$), expression proposed by Antis et al. [18], Evans and Charles [19] and Niihara et al. [20] are used. The equations are

$$\text{Anstis et al.} \quad K_\mathrm{i} = 0.016\left(\frac{E}{H}\right)^{1/2} x \frac{P}{c^{3/2}} \tag{1.4}$$

$$\text{Evans and Charles} \quad K_\mathrm{i} = 0.16H\sqrt{a}\left(\frac{c}{a}\right)^{-3/2} \tag{1.5}$$

$$\text{Niihara et al.} \quad K_\mathrm{i} = 0.0309\left(\frac{E}{H}\right)^{0.4}\left(\frac{P}{c^{3/2}}\right) \tag{1.6}$$

where E is the young modulus, H is the hardness and P is the applied load. For Palmqivst cracks ($c/a \leq 2.5$) expression proposed by Niihara et al. [21] as given below is used

$$K_{\mathrm{i}} = 0.0123E^{0.4}H^{0.1}\left(\frac{P}{l}\right)^{1/2} \tag{1.7}$$

1.6 Tribological Properties

In this section, sliding wear, defined as degradation of coatings due to rubbing of two surfaces in relative motion, erosive wear which is degradation of coatings due to impact of particles travelling with significant velocity and abrasive wear known as material loss when a hard particle is made to slide against a relatively soft-coated surface are addressed. Both forms of sliding wear such as unidirectional sliding wear and reciprocating sliding wear are covered. Erosive wear as a result of liquid drop impact, cavitation erosion, liquid metal, etc., are not discussed. Description of abrasive wear is primarily confined to three body abrasion estimated by rubber wheel abrasive wear test, although high stress abrasion and low stress abrasion are taken into consideration.

1.6.1 Sliding Wear

The most important governing parameters for sliding wear are load and sliding velocity. The influence of load and sliding velocity on coefficient of friction of Cr_3C_2–25(Ni20Cr) coating is presented in Fig. 1.13 [22]. The coefficient of friction increases with increase in applied load. According to Greenwood and Williamson [23], the real contact area is proportional to the normal load. Based on the classical theory of adhesion, the frictional force is defined as [23]:

$$F = \tau_{\mathrm{a}}A_r \quad \text{and} \quad \frac{F}{(L)} = \frac{\tau_{\mathrm{a}}A_r}{(L)} = \mu_{\mathrm{a}} \tag{1.8}$$

where τ_{a} is the average shear strength during sliding and (L) is the applied load. μ_{a} is adhesion induced friction coefficient.

For elastic contact of a spherical indenter and a homogenous half-space, the contact area A_r can be estimated as:

$$A_r = \pi\left(\frac{3(L)R}{4E}\right)^{\frac{2}{3}} \tag{1.9}$$

where E is the effective elastic modulus and R is the effective radius of curvature. Combining Eqs. (1.8) and (1.9), the friction coefficient corresponding to the pure elastic adhesion is given by

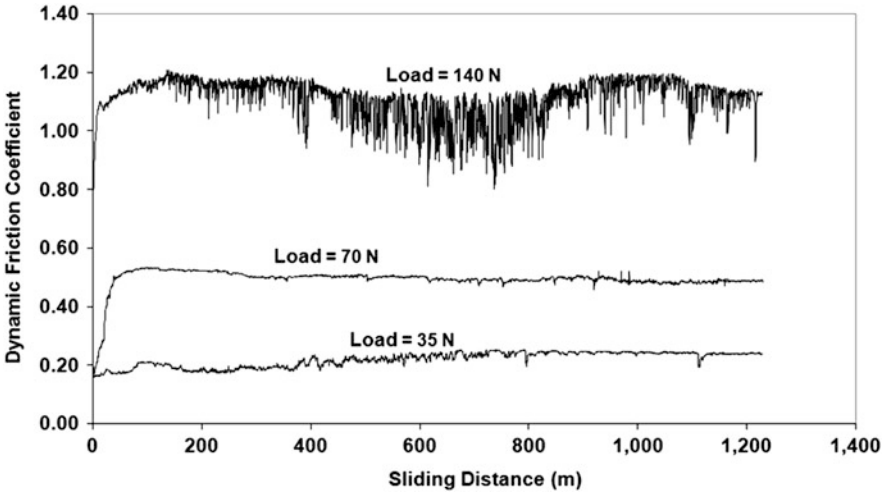

Fig. 1.13 Influence of applied load on the coefficient of friction of HVOF-sprayed Cr_3C_2–25 (Ni20Cr) coating [22]

$$\mu_a = \pi\tau\left(\frac{3R}{4E}\right)^{\frac{2}{3}} L^{-\frac{1}{3}} \tag{1.10}$$

where μ_a is the coefficient of friction, τ is the average shear strength during sliding and L is the applied load. E is the effective elastic modulus and R is the effective radius of curvature. Thus the coefficient of friction is inversely related to the cube root of the applied load and the observation of Fig. 1.13 contradicts this relation. If the adhesion is the dominant friction mechanism, then the coefficient of friction would decrease with the applied load. Thus coefficient of friction in the above observation is not governed by adhesive component.

However, coefficient of friction initially increases with increase in sliding velocity but then remains independent of velocity. Such behaviour is in contradiction of what normally observed and described by the equation given below [24].

$$\mu = K_1 - K_2 \mathrm{Ln}(v) \tag{1.11}$$

where μ is coefficient of friction and v is sliding velocity. K_1 and K_2 are constants. This contrasting behaviour can be attributed to small range of sliding velocity over which the measurement is made. For a wider range of sliding velocity, appropriate relation can be established.

Nanostructured thermal-sprayed coatings are known for their improved wear and friction properties. Conventional and nanostructured WC–12 % Co coatings were deposited on 1Cr18Ni9Ti stainless steel substrate using air plasma spraying by Zhao et al. [25]. The hardness of the coatings was measured, while their friction and wear behaviour sliding against Si_3N_4 at room temperature and elevated

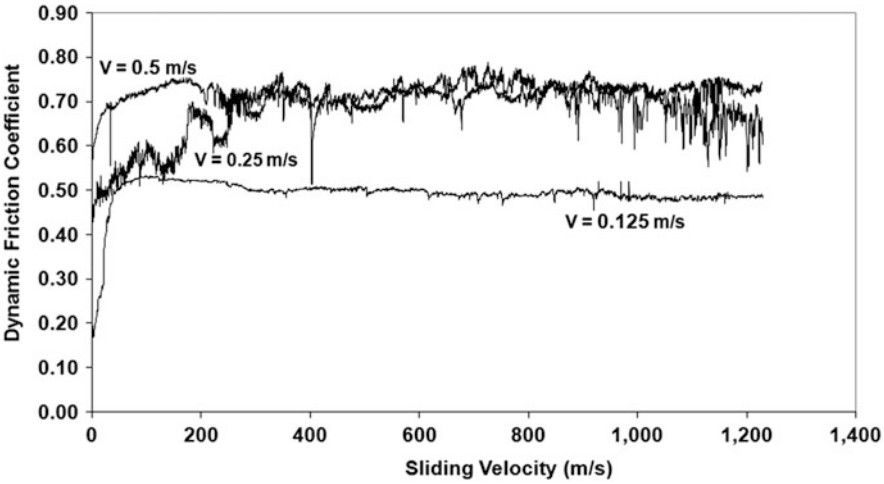

Fig. 1.14 Influence of sliding velocity on the coefficient of friction of HVOF-sprayed Cr_3C_2–25 (Ni20Cr) coating [22]

temperatures up to 673 K were comparatively studied. It was found that the as-sprayed WC–12 % Co coatings were composed of WC as the major phase and W_2C, WC_{1-x}, and W_3Co_3C as the minor phases. The plasma-sprayed nanostructured WC–12 % Co coating had much higher hardness and refined microstructures than the conventional WC–12 % Co coating. This largely accounted for the better wear resistance of the nanostructured WC–12 % Co coating than the conventional coating. Besides, the two types of WC–12 % Co coatings showed minor differences in coefficient of frictions, though the nanostructured WC–12 % Co coating roughly had slightly smaller coefficient of friction than the conventional coating under the same sliding condition as given in Fig. 1.14. Moreover, both the conventional and nanostructured WC–12 % Co coatings recorded gradually increased wear rate with increasing temperature, and the nanostructured coating was less sensitive to the temperature rise in terms of the wear resistance. The nanostructured WC–12 % Co coating with a wear rate as small as 1.01×10^{-7} mm^3/Nm at 673 K could be promising candidate coating for the surface-modification of some sliding components subject to harsh working conditions involving elevated temperature and corrosive medium. The friction behaviour of HVOF-sprayed Cr_3C_2–25 (Ni20Cr) coating having nanocrystalline grains and microcrystalline grains has been studied by Roy et al. [26]. Their work is presented in Fig. 1.15. The coefficient of friction of nanocrystalline grain coating was found to be lower than that of microcrystalline coating. Similar results have been reported by Zhu and Ding [27] for WC–Co coatings.

Thermal-sprayed coatings are extensively used to improve the sliding wear properties of various engineering component. An improvement of wear resistance of mild steel by 200 times by depositing detonation-sprayed WC–12 % Co coating is reported by Roy and Sundararajan [12]. Their work is presented in Fig. 1.16. The

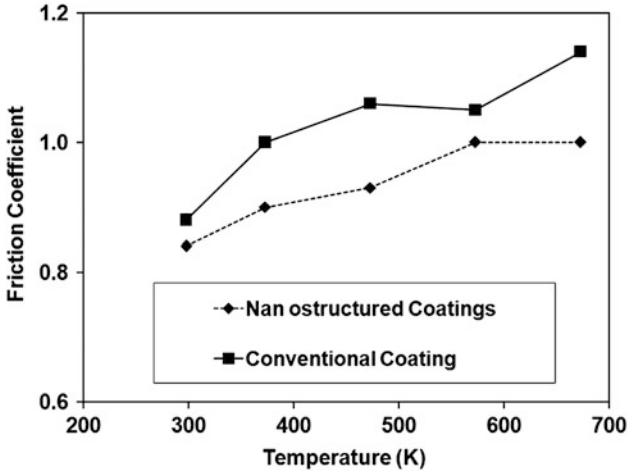

Fig. 1.15 Influence of temperature on the coefficient of friction of plasma-sprayed conventional and nanostructure WC–12 % Co coatings [25]

influence of applied load on wear rate of a NiCrBSi alloy is examined by Rodrıguez et al. [28]. As shown in Fig. 1.17, the load influences the wear rate significantly. However, no specific trend about influence of applied load can be established. Another important thermal-sprayed coating for tribological application is Cr_3C_2–25 (Ni20Cr). The study due to Mohanty et al. [13] indicates that for this variety of coating the wear rate is governed by splats, porosity, forms and distribution of second phase. The coefficient of friction decreases with increase in sliding velocity in accordance with Eq. (1.9). However, wear rate initially decreases with velocity but subsequently increases with sliding velocity. Such behaviour of wear rate can be explained by the fact that at low sliding velocity the wear mechanism is mild oxidational wear and the wear rate in this regime, assuming a flat pin sliding against flat disc, is given by [24, 29]

$$W = \frac{FC^2A_o}{vZ_cH_o} \exp\left(-\frac{Q}{RT_f}\right) \tag{1.12}$$

where A_o is Arrhenius constant, Q is the activation energy for oxidation, F is applied load, H_o is hardness of the oxide scale, Z_c is the critical thickness of spalling, T_f is the temperature at the place of contact of the asperities, v is the sliding velocities, C is a constant which depends on the composition of the oxide scale and R is the molar gas constant. As the velocity term is in denominator, increase in velocity will decrease the expression of Eq. (1.12) and hence the wear rate will decrease. Subsequently when the sliding velocity increases, the wear takes place by severe oxidational wear mechanism. The wear rate in this regime can be given by [24, 29]

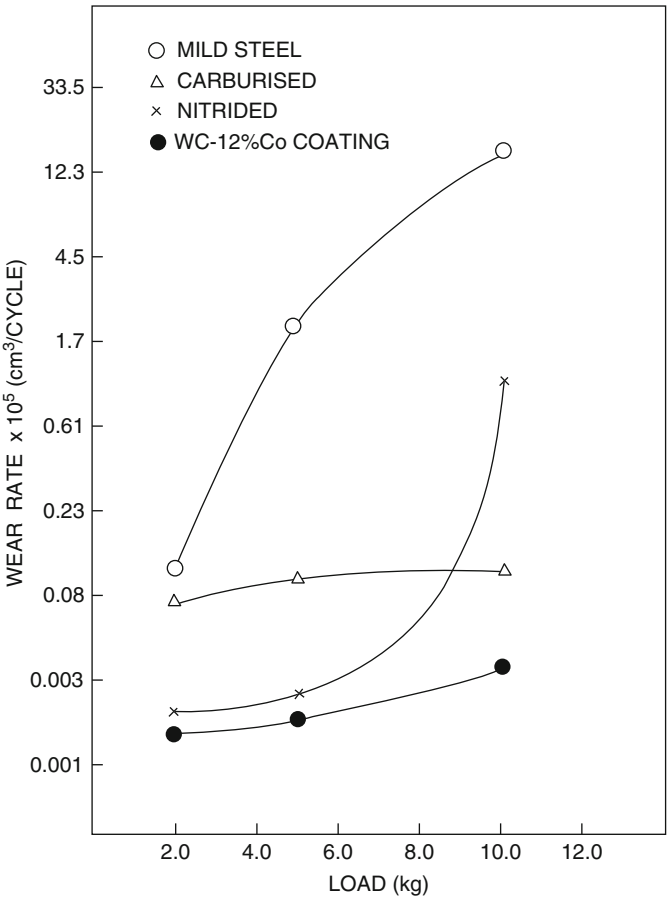

Fig. 1.16 Influence of applied load on the wear rate of detonation-sprayed WC–12 % Co coating, nitrided and carburised mild steel [12]

$$W = \frac{f_{\mathrm{m}}\alpha\mu F}{L_{\mathrm{ox}}} - \frac{f_{\mathrm{m}}K_{\mathrm{ox}}(T_{\mathrm{m}}^{\mathrm{ox}} - T_{\mathrm{b}})F^{1/2}N^{1/2}A_n^{\frac{1}{2}}}{L_{\mathrm{ox}}\beta v r_0 H_{\mathrm{o}}^{1/2}} \tag{1.13}$$

where f_{m} is volume fraction of molten material during sliding, r_0 is the radius of the nominal contact area, L_{ox} is the latent heat for fusion per volume of the oxide scale, β is a dimensionless parameters for bulk heating, N is the total number of asperities, H_{o} is the hardness of the oxide scale, $T_{\mathrm{m}}^{\mathrm{ox}}$ is the melting temperature of the oxide scale, α is the fraction of generated heat that is conducted by the wearing component, μ is friction coefficient, F is applied load, v is sliding velocity and T_{b} the bulk temperature of the wearing material. According to this equation, as sliding velocity increases, the second term of Eq. (1.13) decreases and the wear rate increases.

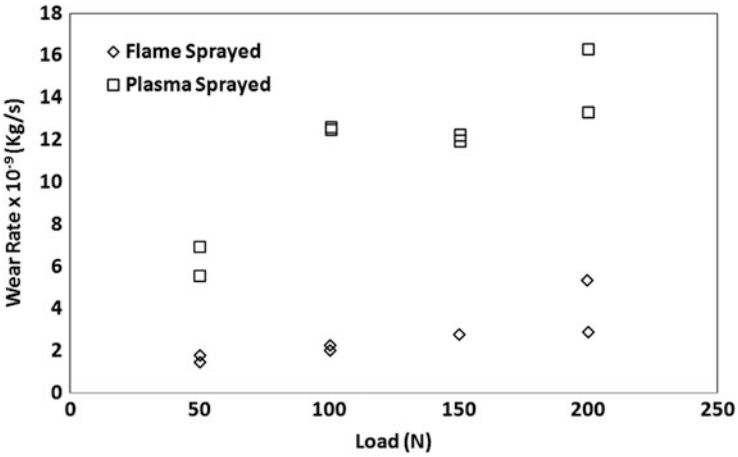

Fig. 1.17 The influence of applied load on wear rate of flame-sprayed and plasma-sprayed NiCrBSi alloy [28]

Wear performance of WC–Co coatings reported to improve significantly by heat treatment [30–32]. Studies by Lenling et al. showed that post-heat treatment of WC base coatings increased the compressive residual stress of these coatings [30]. But research of Stewart et al. [32] showed that heat treatment at all the examined temperatures reduced residual stress of the coating. Increasing of residual stress in thermal spray coatings is very harmful as it may damage the coatings by spalling. On the whole, residual stress is one of the major problems in thermal spray layers especially in thick coatings. Khameneh Asl et al. [33, 34] also found deterioration of tribological properties of WC–Co coatings on heat treatment. Heat treatment also resulted in improvement in wear resistance of Cr_3C_2–25(Ni20Cr) coating as reported by Guilemany et al. [35]. In general, heat treatment improves the wear rate. However, heat treatment at 1,033 K for 1 h in inert atmosphere improves the wear rate dramatically. This happens due to precipitation of Cr_3C_2 in Ni20Cr matrix. During heat treatment in oxidising atmosphere, Cr combines with oxygen and forms Cr_2O_3. This is minimised in inert atmosphere and thus exhibiting best wear performances. Stoica et al. [36] deposited functionally graded WC–NiCrBSi coatings by thermally sprayed using a high velocity oxyfuel (JP 5000) system and heat treated at 1,473 K in argon environment. The relative performance of the as-sprayed and heat-treated coatings was investigated in sliding wear under different tribological conditions. Results indicate that by heat treating the coatings at a temperature of 1,473 K, it is possible to achieve higher wear resistance, both in terms of coating wear, as well as the total wear of the test couples. This was attributed to the improvements in the coating microstructure during the heat treatment and this resulted in an improvement in coating's mechanical properties through the formation of hard phases, elimination of brittle W_2C and W and the establishment of metallurgical bonding within the coating microstructure.

Post-coating treatments other than heat treatment do alter the wear behaviour. Hipping is one such process which results in improvement of wear rate as noted by Stoica et al. [37]. The relative performance of the as-sprayed and hot isostatically pressed functionally graded WC–NiCrBSi coatings was investigated in sliding wear conditions. Coatings were deposited using a high velocity oxy-fuel (HVOF) JP 5000 system and HIPed without any encapsulation at temperatures of 1,123 and 1,473 K. The results indicated significant alteration of the coating microstructure, brought about by the coating post-treatment, particularly when carried out at the higher temperature of 1,473 K. As a consequence, improvements in the coating mechanical properties took place that led to higher wear resistance of the HIPed coatings. They have also examined effect of hipping on WC–Co coating [38]. WC–12Co coatings sprayed by a HVOF system were deposited on SUJ-2 bearing steel substrate and then encapsulated and HIPed at 1,123 K for 1 h. Hot isostatic pressing of thermal spray coatings was seen to improve the microstructural features by reducing porosities and increasing intersplat bond strength, physical properties, and, correspondingly the wear resistance of cermet coatings. As a result, the wear resistance of the post-treated coatings was approximately twice that of the as-sprayed coatings as shown in Fig. 1.18. Hipping resulted in elimination of secondary phase W_2C and metallic tungsten W, alteration of amorphous binder phase through recrystallisation of Co leading to precipitation of the η carbides and development of metallurgical bonding at the interface between the constituent lamellae of the coating, thereby increasing the coatings modulus after HIPing. Wear mechanism of as-sprayed coatings, which lost higher amounts of material, is by microcracking, spallation, ploughing and material transfer. The wear mechanisms involved in the HIPed coating/ball test couples were extrusion of binder followed by the removal of the carbide grains, some levels of abrasion, plastic deformation and material transfer. Similarly Mateos et al. [39] found improvement of wear rate of plasma-sprayed Cr_3C_2–25(Ni20Cr) coating by laser glazing. Laser glazing made the coating more homogeneous, free from porosity, harder and improved adhesion. This in turn resulted in improve wear rate.

Bolelli et al. [40] produced Al_2O_3 coatings by the high-velocity suspension flame spraying (HVSFS) technique using a nanopowder suspension. Their structural and microstructural characteristics, micromechanical behaviour and tribological properties were studied and compared to conventional atmospheric plasma-sprayed and high-velocity oxygen-fuel-sprayed Al_2O_3 coatings manufactured using commercially available feedstock. The HVSFS process enables near full melting of the nanopowder particles, resulting in very small and well-flattened lamellae (thickness range 100 nm to 1 μm), almost free of transverse microcracking, with very few unmelted inclusions. Thus, porosity is much lower and pores are smaller than in conventional coatings. Moreover, few interlamellar or intralamellar cracks exist, resulting in reduced pore interconnectivity (evaluated by electrochemical impedance spectroscopy). Such strong interlamellar cohesion favours much better dry sliding wear resistance at room temperature as described in Fig. 1.19.

The kind of fuel used also governs wear performances. Work due to Sudaprasert et al. [41] as presented in Fig. 1.20 indicates that wear rate of WC–12 % coating

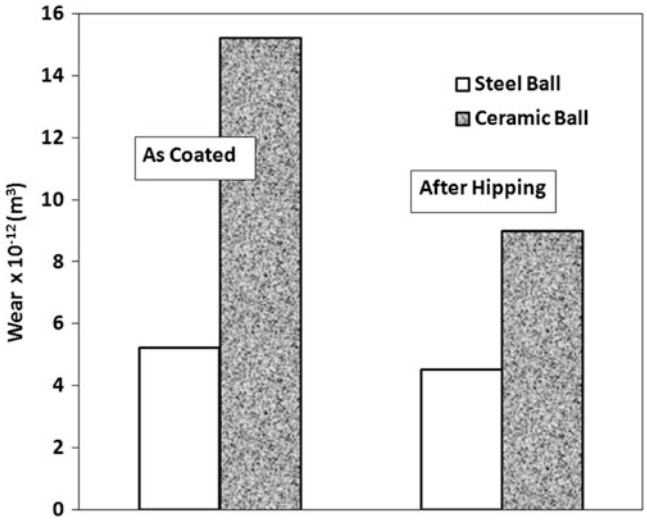

Fig. 1.18 The influence of hipping on the wear of HVOF-sprayed WC–Co coating [38]

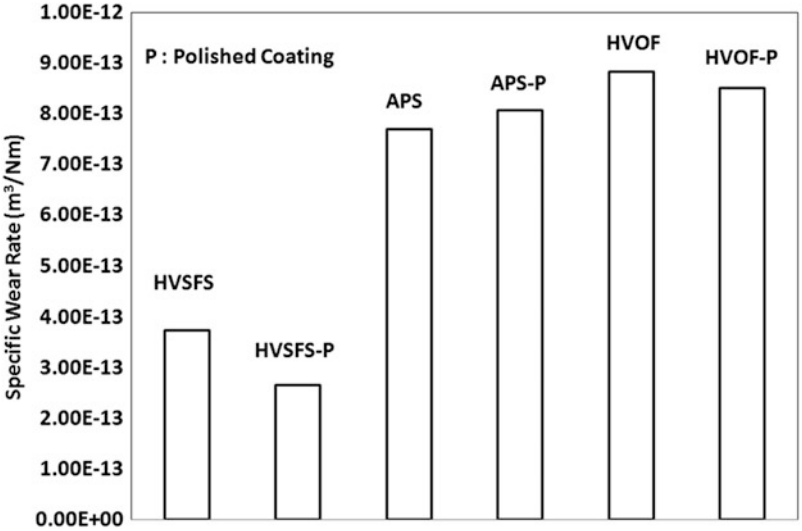

Fig. 1.19 The influence of spraying techniques on the wear rate of Al_2O_3 coatings in as-received and polished condition deposited by high velocity suspension flame (HVSFS), HVOF and air plasma spraying [40]

increases as oxy gaseous fuel is changed to oxy liquid fuel. During spraying with gaseous fuels, the binder material is totally molten and carbide dissolution is extensive forming a highly alloyed matrix. On impacting, binders solidify leaving well-bonded carbides with the matrix phase. In contrast, during liquid fuel spraying,

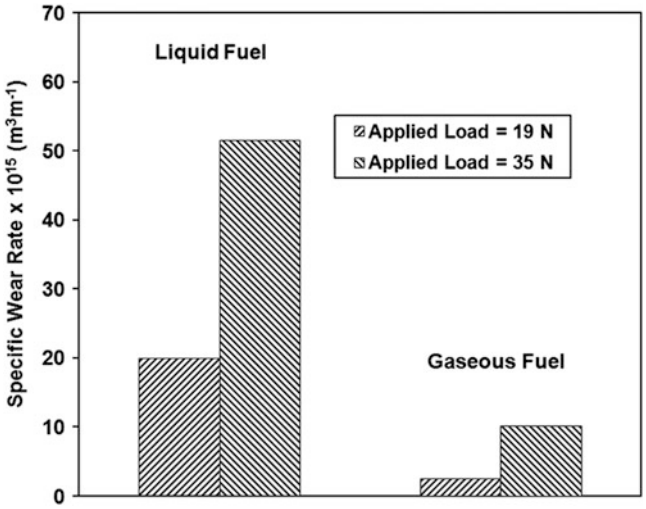

Fig. 1.20 The influence of type of fuel on the wear rate of HVOF-sprayed WC–Co coating [41]

binder is partially molten leaving solid core and liquid shell. On impact the solid core are damaged. This leads to poor wear resistance.

In recent times WC–Co–Cr powders are employed to improve wear and corrosion resistance [42–45]. Addition of Co to Cr results in improvement of adhesion of the WC particles with the matrix [46]. Lee et al. [45] noted that the mixing of fine and coarse powders results in improvement of mechanical and tribological properties. Their observation shown in Fig. 1.21 indicates best wear resistance for mixed powder containing 70 % fine powder and 30 % coarse powders. This observation is attributed to the fact that spaces generated by insufficient melting of coarse powders are filled by large amount of molten fine powders.

Counterbody governs the wear resistance to a significant extent. Mechanically alloyed Al–12Si/TiB_2/h-BN composite powder was deposited on aluminium substrates by atmospheric plasma spraying by Ozdemir et al. [47]. It has been observed that TiB_2 and in situ formed AlN and Al_2O_3 phases in combination with h-BN solid lubricant strongly affect the wear performance of the coating. The presence of solid lubricant, h-BN (7.7 wt.%), had no significant influence in reducing the coefficient of friction of the plasma-sprayed coatings as compared to the that of the substrate. Counter material plays an important role in reducing the volume loss of the coatings after wear test. The volume loss of the coating was measured approximately two times higher when it was wear tested against Al_2O_3 ball instead of 100Cr6 ball as illustrated in Fig. 1.22.

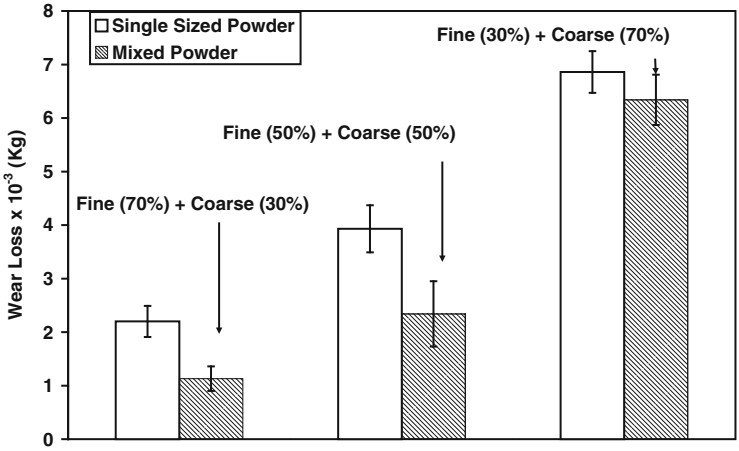

Fig. 1.21 Influence of powder mixing on the wear rate of HVOF-sprayed WC–10Co–4Cr coating [45]

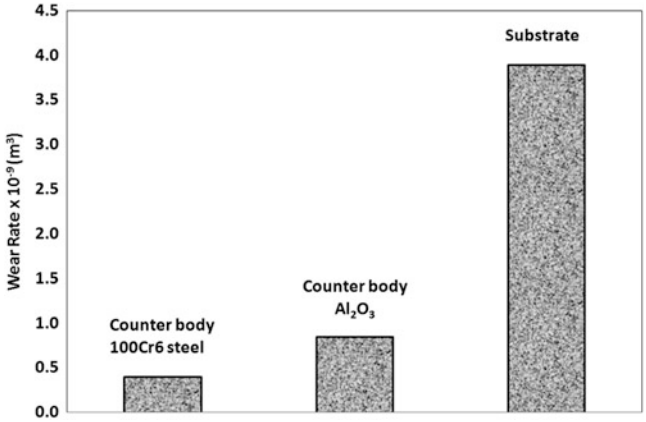

Fig. 1.22 Influence of counterbody material on the wear rate of Al–12Si/TiB_2/h-BN composite coating [47]

1.6.2 Erosive Wear

Thermal-sprayed coating is extensively used for protection against erosive wear as well. In order to examine what is the most erosion resistance thermal-sprayed coating, work of Hawthorne et al. [48] appears to be the most relevant. The performance of ten high velocity oxy-fuel HVOF-sprayed coatings has been evaluated under normal and oblique impingement conditions. Their results are presented in Fig. 1.23. Erosion test was conducted with 50 mm quartz particles at an impact velocity of 84 m/s. It is clear that WC–Co coating has the highest erosion

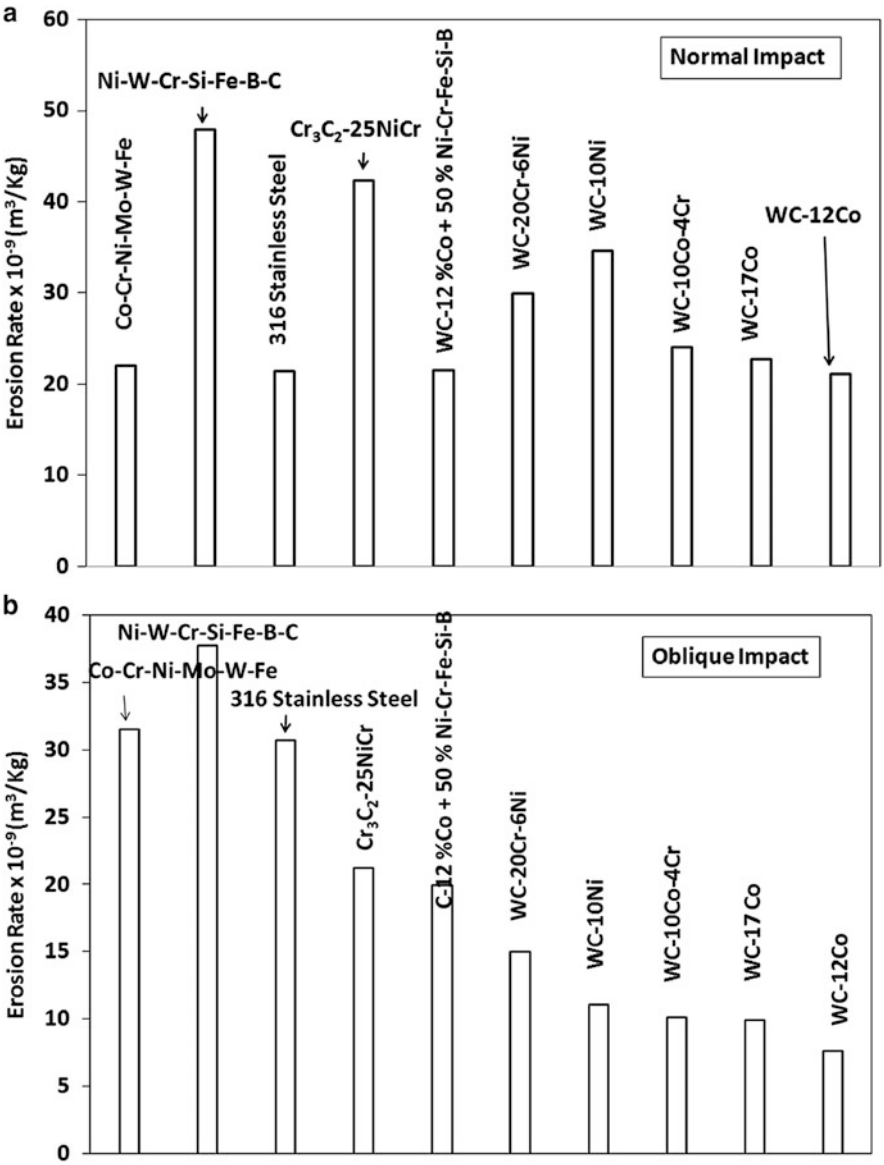

Fig. 1.23 The erosion rate of various thermal-sprayed coatings [48]

resistance. For this coating, material loss was by cutting, platelet removal and occasionally by carbide particle removal. Levy and Wang [49] noted brittle erosion response characterised by lower erosion rate at oblique impact than at normal impact of plasma-sprayed WC–Co coating. Observation of Barbezat et al. [50] indicated CDS-sprayed WC–Co coating exhibits improved erosion resistance.

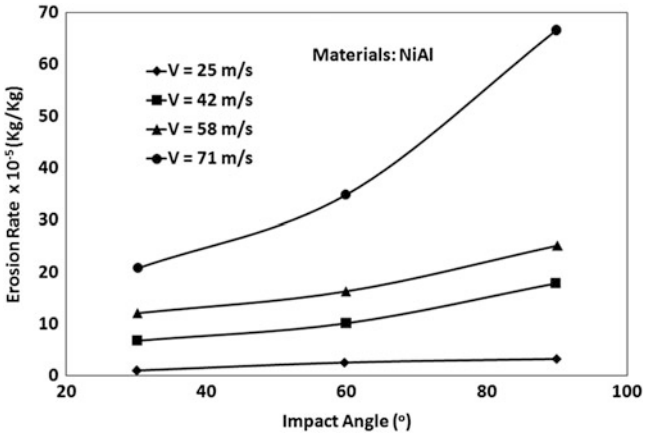

Fig. 1.24 The influence of impact angle on the erosion rate of HVOF-sprayed NiAl coating [54]

Impact angle independent erosion rate at low impact velocity and impact angle dependent erosion rate at high impact velocity for WC–Co coating is noted by Wood et al. [51]. As reported by Karimi et al. [46], addition of Co to Cr results in improvement of adhesion of WC particles with the matrix resulting in improved erosion resistance. According to Kim et al. [52] erosion rate of plasma-sprayed WC–Co coating decreases with increase of cohesive strength. Roy et al. [53] demonstrated that the erosion resistance of detonation-sprayed WC–Co coating is better than plasma-sprayed and HVOF-sprayed coatings at normal impact and comparable at oblique impact.

The influence of erosion conditions on the erosion resistance can be noted from the work of Hearley et al. [54]. The influence of impact angle on the erosion rate of HVOF-sprayed NiAl coating can be seen from Fig. 1.24. Erosion rate is maximum at normal impact indicating classical brittle erosion response. However, examination of eroded surfaces indicates ductile materials removal mechanism. Materials removal is governed by deformation rather than fracture. This apparent contradictory behaviour lies on the nature of erodent, their size and shape. They also showed the effect of impact velocity on erosion response of HVOF-sprayed NiAl coating. Their result, shown in Fig. 1.25, indicates increase of erosion rate with increase of impact velocity. Relation between erosion rate and impact velocity for this type of behaviour can be obtained from the following expression:

$$E \infty V^{3.2} r^{3.7} \rho^{1.3} H^{-1.25} \tag{1.14}$$

where V is impact velocity, r is radius of the erodent and ρ and H are density and hardness of target material.

Influence of test temperature on erosion rate is studied by Wang and Verstak [55] as shown in Fig. 1.26. The target materials used for the erosion test were the HVOF-sprayed Cr_3C_2/TiC–NiCrMo cermet produced with a self-propagating high-

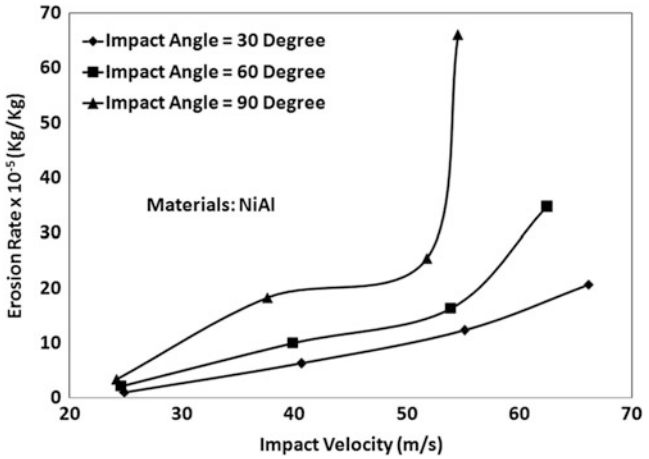

Fig. 1.25 The influence of impact velocity on the erosion rate of HVOF-sprayed NiAl coating [54]

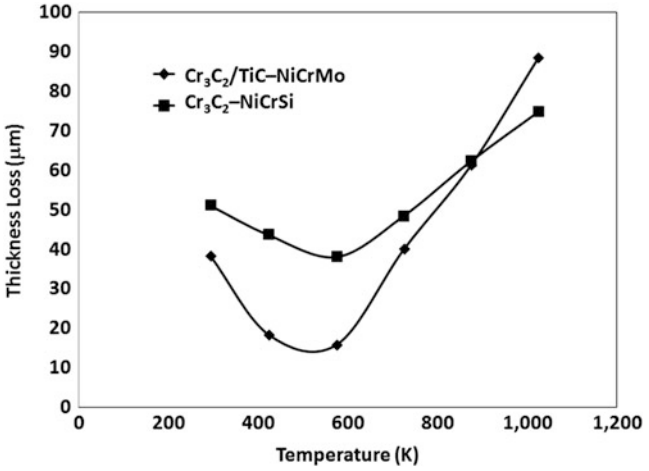

Fig. 1.26 The influence of test temperature on the erosion rate of HVOF-sprayed Cr_3C_2/TiC–NiCrMo cermet coatings [55]

temperature synthesis method [56, 57] and blended Cr_3C_2–NiCrSi cermet coatings on mild steel. The coating was sprayed using the Sulzer-Metco Diamond Jet spray system. Propane was used as a fuel gas. It is observed that the thickness loss decreased in the range from room temperature to 673 K and then increased in the range from 673 to 1,023 K. Similar results for alumina and zirconia plasma-sprayed coatings have been reported in the literature [58]. It is evident that the erosion behaviour of the HVOF Cr_3C_2/TiC–NiCrMo coating is more sensitive to temperature than that of the HVOF Cr_3C_2–NiCrSi coating. Below 873 K the thickness loss

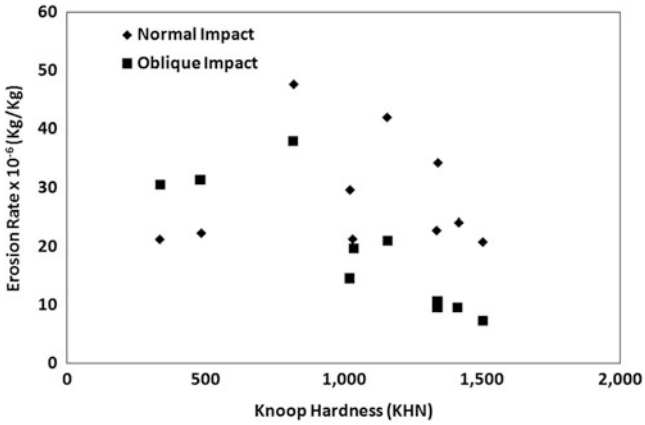

Fig. 1.27 The influence of hardness on the erosion rate of thermal-sprayed cermet coatings [48]

of the HVOF Cr_3C_2/TiC–NiCrMo coating was lower than that of the HVOF Cr_3C_2–NiCrSi coating. Yet with increasing temperature, the thickness loss of the former increased faster than the latter. Over 873 K the erosion wastage of the HVOF Cr_3C_2/TiC–NiCrMo coating was even higher than that of the HVOF Cr_3C_2–NiCrSi coating. The higher sensitivity of the HVOF Cr_3C_2/TiC–NiCrMo coating to temperature may be related to oxidation of titanium carbide TiC. Therefore, the HVOF Cr_3C_2/TiC–NiCrMo coating is not suitable for applications under such high temperatures.

Work of Hawthorne et al. [48] also exhibited the influence of hardness on the erosion rate of thermal-sprayed coatings. As shown in Fig. 1.27, there is no direct correlation between hardness and erosion rate. However, at normal impact there is a tendency for decrease of erosion rate with increase of hardness. The lamellar structure determines the mechanical properties of thermal-sprayed coatings. Li et al. [59] measured the erosion rate of plasma-sprayed Al_2O_3 coating under normal impact condition. They derived a microstructural parameter mean bonding ratio between lamellae and thickness of the lamellae. The result shown in Fig. 1.28 clearly indicates that the erosion resistance is inversely proportional to the mean bonding ratio. They were able to establish the relation as given below:

$$\frac{1}{E} = \frac{2\gamma_c \alpha}{E_{\text{eff}} \delta} \tag{1.15}$$

where γ_c is the effective surface energy of the lamella material, α is the bonding ratio of the interface between lamellae, δ is the thickness of the lamella, $1/E$ is the erosion resistance and E_{eff} is the fraction of kinetic energy per unit mass of impacting particle utilised for cracking of the bonded lamellar interface.

The post-coating treatment also alters the erosion performances of coatings. Tsai et al. [60] investigated the improvement of erosion resistance of plasma-sprayed

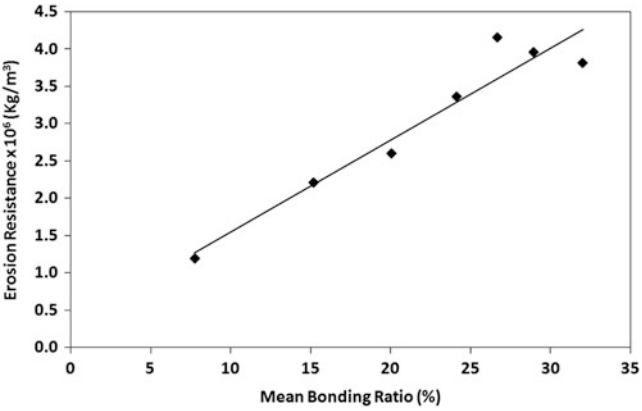

Fig. 1.28 The influence of mean bonding ratio between lamellae and thickness of the lamellae on the erosion rate of plasma-sprayed Al_2O_3 coating [59]

thermal barrier coatings on laser glazing. Several erosion tests were conducted at room temperature using 50 μm silica erodent particles with impact velocity of 50 m/s. The erosion rate increased as the impingement angle increased for both plasma-sprayed and laser-glazed TBC. Laser glazing enhanced the erosion resistance of plasma-sprayed TBC by about 1.5–3 times with the impingement angle ranging between 30 and 75°, while the erosion resistance did not significantly improve when the impingement angle reached 90° as shown in Fig. 1.29. Erosion morphology analysis clearly indicates that the erosion of the plasma-sprayed TBC is deemed to be the erosion of the protrusions and the sprayed splats. The erosion of the laser-glazed TBC is proven to be the spallation of the glazed layer. Spallation occurred in the laser-glazed layer/plasma-sprayed splats interface. Similarly the nature of coating materials also reflects the performance under erosion condition. The investigation due to Kulu et al. [61] presented in Fig. 1.30 indicates that WCCoCr coating has significantly lower erosion rate than self fluxing NICrSiB coating.

A series of hot erosion and erosion–corrosion (E–C) tests was carried out on thermal-sprayed coatings, diffusion coatings and boiler steels using a burner-rig type elevated temperature E–C tester by Uusitalo et al. [62]. Carbide containing HVOF coatings, diffusion coatings and nickel-based high-chromium HVOF coatings performed well. A series of elevated temperature erosion tests was carried out on AlSl 1018 low-carbon steel and four thermal spray-coated mild steel specimens using a nozzle-type elevated temperature erosion tester by Wang and Lee [63]. The thermal-sprayed coatings included a high velocity oxy-fuel (HVOF) $75Cr_3C_2$–20NiCr cermet coating, HVOF Cr_3C_2 low velocity flame-sprayed Cr_3C_2, ceramic coatings and an arc-sprayed Fe–CrSiB coating. The HVOF Cr_3C_2, coating specimen exhibited the lowest erosion wastage due to its favourable composition and morphology. It had a finer structure and smaller splat size than other coatings. Guilemany et al. [64] successfully sprayed the near stoichiometric Fe40Al by

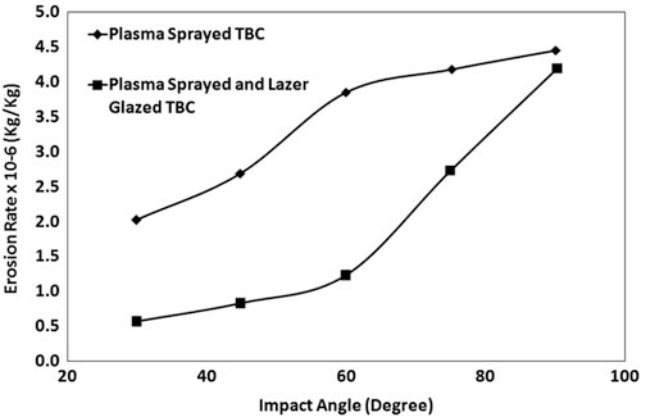

Fig. 1.29 The improvement of erosion resistance of plasma-sprayed thermal barrier coatings on laser glazing [60]

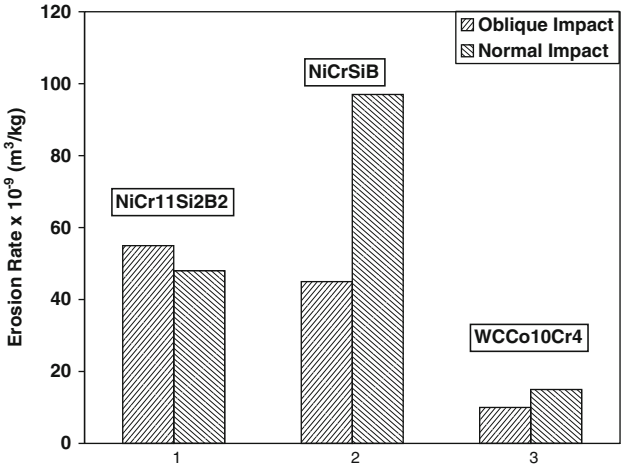

Fig. 1.30 Higher erosion resistance of WCCo10Cr4 coating than self-fluxing NiCr11Si2B2 coating [61]

means of high velocity oxy-fuel. Erosion tests demonstrated that iron aluminides possess a ductile behaviour even when the impingement angle is 90°.

Unlike sliding wear, the work on solid particle erosion of nanocomposite coatings is very less. Only work due to Dent et al. [65] indicates that erosion resistance of nanocomposite coating decreases compared to conventional coatings. However, in nanostructure coating, erosion resistance increases with decrease in Co binder phase.

1.6.3 Abrasive Wear

Most important thermal-sprayed coatings other than WC–Co that are used against abrasion are Al_2O_3, TiO_2, Cr_2O_3, etc. [66, 67]. According to Liu et al. [68], the abrasive wear resistance of thermal spray coating can empirically be related to hardness and indentation toughness of the coating as given below:

$$\mathrm{WR}_{\mathrm{abrasion}} = C\frac{H^{1/2}K^{2/3}}{(1+nP)} \tag{1.16}$$

where H is hardness, K is indentation toughness, P is porosity, n is a parameter to be determined experimentally and C is a constant. The results of Habib et al. [69] which shows the influence of hardness on abrasive wear resistance is given in Fig. 1.31. It can be seen that abrasive wear resistance is directly related to the hardness of the coating and toughness and porosity have minimum influence. Work due to Kim et al. [52] exhibited decrease of abrasive wear rate with increase of bond strength. A systematic study by Barbezat et al. [50] indicated that under three body abrasion WC–12 % Co coating exhibited lower abrasion rate than WC–17 % Co coating. For WC–12 % Co coating, abrasion resistance was maximum for coating obtained by continuous detonation spraying whereas for WC–17 % Co coating abrasion was maximum for coating obtained by cyclic detonation spraying. It is to be stated that minimum abrasion resistance can be seen for coating obtained by vacuum plasma spraying for both variety of coatings. This observation was attributed to inter splat adhesion strength. Nerz et al. [70] demonstrated that abrasive wear resistance of high energy plasma-sprayed or HVOF-sprayed WC–Co coating increases when the coating was heat treated above recrystallisation temperature due to formation of various hard carbides.

When a hard phase is uniformly distributed in a soft phase using quantitative metallography, Lee and Gurland [71] proposed following equation to estimate grain sizes and contiguity of hard phase and binder mean free path:

$$d_{\mathrm{WC}} = \frac{2V_{\mathrm{WC}}}{2N_{\alpha\alpha} + 2N_{\alpha\beta}} \tag{1.17}$$

$$C_g = \frac{2N_{\alpha\alpha}}{2N_{\alpha\alpha} + N_{\alpha\beta}} \tag{1.18}$$

$$\lambda = \frac{d_{\mathrm{WC}}(1 - V_{\mathrm{WC}})}{V_{\mathrm{WC}}(1 - C)} \tag{1.19}$$

where d_{WC} is the tungsten carbide grain size, C_g is the contiguity of tungsten, λ is the binder mean free path, V_{WC} is the volume fraction of tungsten carbide, $N_{\alpha\alpha}$ is the average number of intercepts per unit length of test line for carbide–carbide

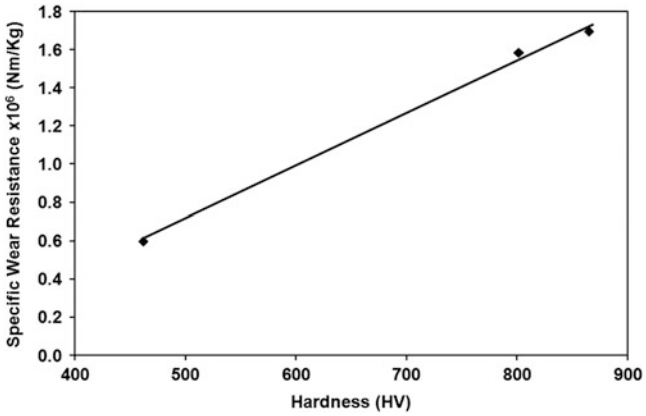

Fig. 1.31 The influence of hardness on abrasive wear resistance of ceramic layers of Al_2O_3/TiO_2 deposited by flame spray [69]

intercepts and $N_{\alpha\beta}$ is the average number of intercepts per unit length of test line for carbide binder intercepts. An interesting study was reported by Kumari et al. [72]. According to their observation shown in Fig. 1.32, the abrasive wear rate of WC–10Co–4Cr coating deposited by JP 5000 gun increased with increase of mean free path of the carbides. As materials loss takes place primarily by abrasion of binder followed by pulling out of carbide particle, binder abrasion becomes difficult due to small mean free path as the abrasive directly interact with hard carbides.

Post-coating heat treatment can alter abrasive wear rate significantly. Stewart et al. [73] sprayed WC–17 wt.% Co powders by the HVOF method to form coatings approximately 200 μm thick on steel substrates. Analysis of the microstructure of the coatings found to consist of WC, W_2C and anamorphous binder phase. Some of the carbide particles are found to decarburise and dissolve in the liquid metal binder during spraying, resulting in a brittle binder phase in the coating. The coatings also exhibit tensile stresses in the as-sprayed condition. Coatings have been heat treated at a range of temperature between 523 and 1,373 K. Heat treatment above 873 K resulted in significant phase changes with in the coating. However, heat treatment at all the temperatures resulted in changes in the integrity and residual stress state of the coating due to thermal expansion coefficient mismatch between the coating and substrate. The abrasive wear behaviour of the as-sprayed and heat-treated coatings demonstrates that heat treatment improves the wear behaviour. Heat treatment at temperature as low as 573 K has resulted in improvement in wear resistance up to 35 %.

The constituents of spraying feedstock play an important role in determining abrasive wear resistance. Wang et al. [74] studied the abrasive wear performance of coatings deposited by high velocity oxy-fuel (HVOF) thermal spraying using of multimodal and conventional feedstocks. WC–12Co coatings were deposited under same conditions using multimodal and conventional WC–12Co powder feedstocks.

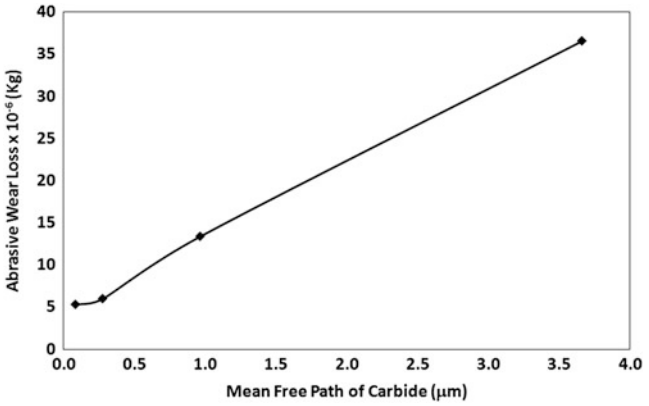

Fig. 1.32 The influence of mean free path of the carbides on the abrasive wear rate of WC–10Co–4Cr coating deposited by JP 5000 gun [72]

Abrasive wear resistances of coatings were carried out on sand rubber wheel abrasion tester. The results shown in Fig. 1.33 indicated the multimodal coating showed better abrasive wear resistance than the conventional counterpart. Also, the thermally sprayed carbide-based coatings have excellent wear resistance with respect to the hard chrome coatings. The nanophase WC–Co component in the multimodal material melts with relative ease and forms a strong and tough matrix that holds the coarse WC particles in place. In turn, the coarse particles provide a hard, 'blocky' surface that is needed for good wear resistance. According to Sudaprasert [41], the dense conventional powder will tend to result in fracture of the carbides on impact, whereas the more porous multimodal powder will cushion impact and result in better wear resistance. Wirojanupatump et al. [75] also studied the influence of powder feedstock on abrasive wear rate of Cr_3C_2–25(Ni20Cr) coating. They deposited the coating using 'Miller Thermal' top gun employing three different types of feedstocks namely sintered and crushed powder, blended powder and composite powder. Sintered and crushed powder was produced by furnace route to give Cr_3C_2 with NiCr metallic binder. Blended powder was prepared by gas atomising NiCr alloy with Cr_3C_2. Composite powder was supplied by 'Praxair' and prepared through a series of thermal and chemical reaction to obtain a fine grain carbide dispersed in a metal matrix. The coating obtained using composite powder feedstock exhibited best abrasion resistance as it has highest hardness due to high degree of carbide retention and small degree of reaction of these particles during spraying.

The influence of amount of reinforcement on the abrasive wear behaviour can be found in the work of Gawne et al. [67]. A ball-milled mixture of glass and alumina powders has been plasma sprayed to produce alumina–glass composite coatings. The coatings have the unique advantage of a melted, ceramic secondary phase parallel to the surface in an aligned platelet-like composite structure. The alumina raises the hardness from 300 HV for pure glass coatings to 900 HV for a 60 wt.%

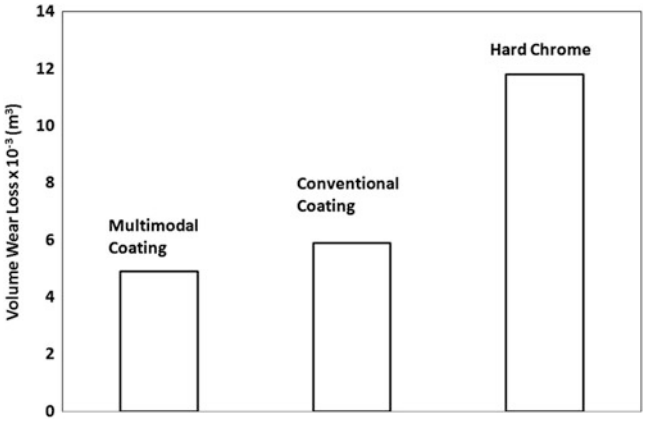

Fig. 1.33 The influence of multimodal and conventional feedstocks on the abrasive wear rate of HVOF-sprayed WC–12 % Co powder [74]

alumina–glass composite coating. The scratch resistance increases by a factor of 3, and the wear resistance increases by a factor of 5. The variation of wear resistance with the amount of reinforcing alumina is shown in Fig. 1.34. Such variation follows the expression provided by Zum Ghar and Eldis [76] as given below:

$$\frac{1}{W} \infty \frac{d^{3/2} v}{\lambda} \tag{1.20}$$

where W is the wear resistance, d is mean diameter of reinforcing particles, v is the volume fraction of reinforcing particles and λ is the mean free path of the particles in the matrix. Thus wear resistance increases with increase in volume fraction of reinforcing particles. The wear resistance reaches a maximum at 40–50 vol.% alumina, above which there is little further improvement. The glass wears by the formation and intersection of cracks, while the alumina wears by fine abrasion and supports most of the sliding load.

Micro-abrasion–corrosion of detonation-sprayed WCCoCr samples in alkaline solutions for different sliding distances as reported by Thakare et al. [77] show generation of a negative synergy that increases with increasing sliding distance. Corrosion takes place at the binder–carbide interface in a region which is likely to have a composition of W_2C. The localised corrosion observed along the carbide grain boundary is due to the corrosion of the decarburised surface of the carbide grain which progresses towards the carbide grain centre and not into the binder phase. Anodic treatment of the WC–Co–Cr samples shows a mild negative synergy. Such treatment has not replicated the wear–corrosion processes seen for the exposed samples. A non-linear relationship between the abrasion–corrosion specific wear rate and E_{corr} is seen and is related to subtle changes in the surfaces such as the formation of passive films during exposure which are not formed during the anodic treatments. Despite the fact that mechanical abrasion losses dominate the

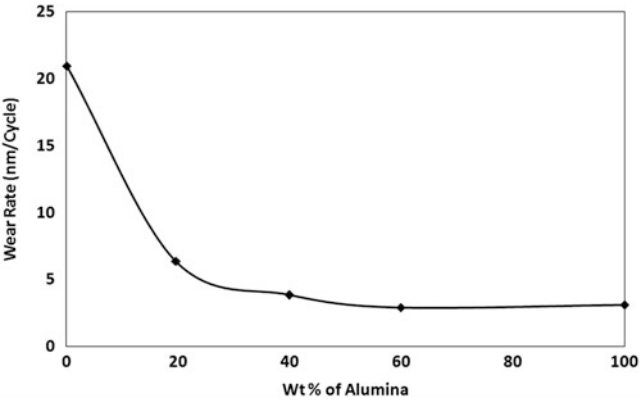

Fig. 1.34 The influence of volume fraction of reinforcing alumina on plasma-sprayed alumina–glass composite coatings [67]

abrasion–corrosion processes, negative synergies are seen due to corrosion which only accounts for 1/500th of the material loss.

Nanocomposite WC–Co coatings are also received attention for abrasive wear related application. However, unlike sliding wear, nanocomposite coating exhibited lower abrasion resistance than conventional coatings [78] due primarily to the decarburisation of wear-resistant WC particles and formation of amorphous phases. Similar behaviour is also noted by Dent et al. [65] although they found that abrasive wear resistance increases with decrease in Co binder content as shown in Fig. 1.35. The abrasive wear rate of nanocomposite coating is also found to be superior to microcrystalline coatings although they are sensitive to the size of abrasives as presented in Fig. 1.36 [79]. In this study, the abrasive wear behaviour of nanocrystalline coatings of the composition (Ti, Mo)(C, N)–45 vol.% NiCo, prepared by vacuum plasma spraying (VPS) of high-energy-milled powder, is characterised and compared to microcrystalline coatings of the same composition. Two-body abrasive wear tests are applied to produce wear traces on the surfaces of the nano- and microcrystalline coatings. Nanocrystalline VPS coatings show superior wear resistance. The wear mechanisms and failure of nano- and microcrystalline coatings are distinctly different.

The potential of post-spraying heat treatment for improving the wear properties of WC–Co nanocomposite coatings has been investigated by Kim et al. [80]. Heat treatment of the coating at 873 K provided an improvement in abrasive wear resistance by 45 %, with an increase in microhardness of the coating as shown in Fig. 1.37. Microstructural examinations showed that heat treatment promoted the formation of additional carbide phases in the splat boundary layer. This increased carbide volume fraction made a major contribution to the improved coating performance. However, higher heat treatment temperatures above 1,073 K reduced the volume fraction of WC and W_2C phases, resulting in detrimental effects on microhardness and abrasive wear resistance of the coatings. Jordan et al. [81] and

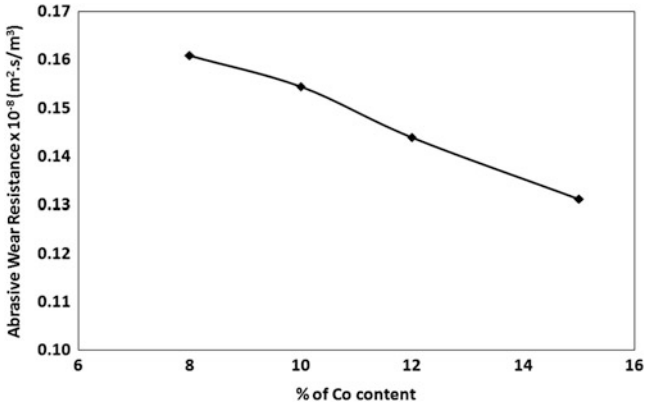

Fig. 1.35 The influence of Co content on abrasive wear resistance of thermal-sprayed WC–Co coatings [65]

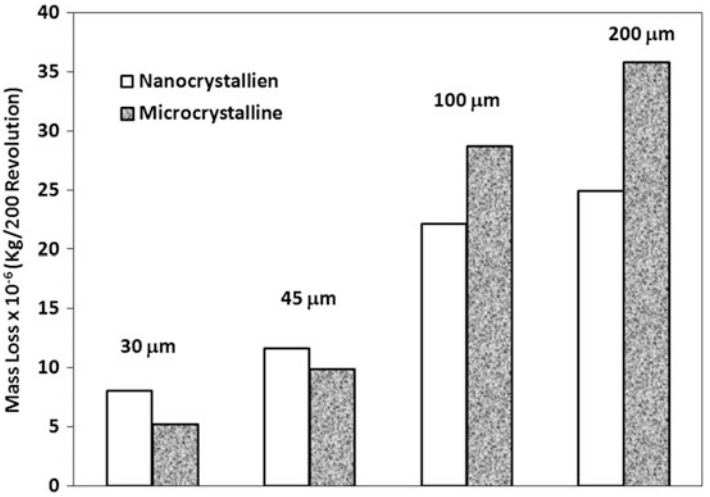

Fig. 1.36 The influence of size of abrasives on the abrasive wear resistance of nanocomposite and microcrystalline vacuum plasma-sprayed (Ti, Mo)(C, N)–45 vol.% NiCo coatings [79]

Gell et al. [82] also found improvement of abrasive wear resistance of nanostructured alumina–titania coatings by modifying the powder with addition of nanostructured oxide powder followed by heat treatment at high temperature (1,073–1,473 K).

Nanocomposite coatings are extremely popular in recent time for tribological application. The mechanical and tribological properties of nanocomposite WC–Co coating can be improved if carbide powders are coated with cobalt. In a study by Baik et al. [83], a porous spray-dried WC–Co nanocomposite powder has been modified by a protective Co surface layer and then sprayed onto a substrate by high

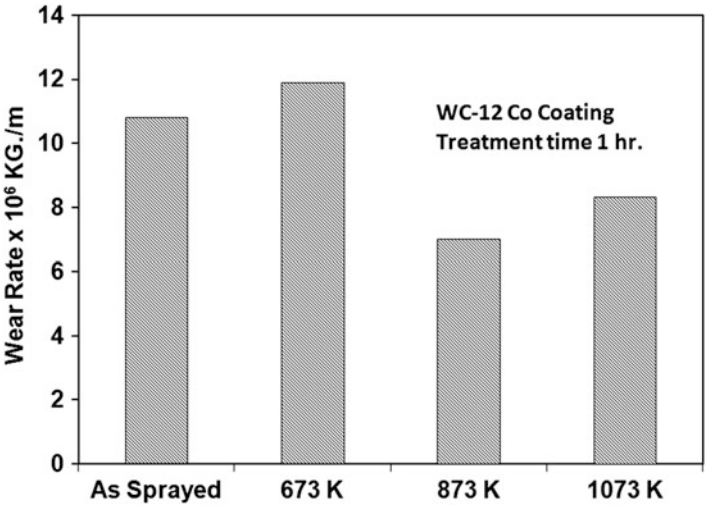

Fig. 1.37 The influence of post-coating heat treatment temperature on the abrasive wear rate of HVOF-sprayed WC–12 % Co coating [80]

velocity oxy-fuel to form a coating. The Co-coated powder promoted coarser size of splats, lower degree of WC decomposition and higher retained carbon content in the coating, compared to the spray-dried powder, mainly because of a limited powder melting. Improvements in hardness and abrasive wear resistance were obtained from the Co-coated powder coating, and the results depicted in Fig. 1.38 are attributed to more retained WC and consequently a lower amount of non-WC phases whose presence is detrimental to wear resistance.

1.7 Applications of Thermal-Sprayed Coatings

Figure 1.39 shows an application of WC–Co coating in aircraft engine. The internal coating of stage III disc of an aircraft engine is illustrated in this figure. With this coatings disc, life is reported to increase substantially. There are of course numerous other applications where WC–Co coatings are applied to protect the components from tribological degradation. Similarly, thermal-sprayed WC–Co coated mixer impeller and electric arc-sprayed stainless steel coated in tapered centre portion of forged lifting lid is shown in Fig. 1.40a and Fig. 1.40b, respectively.

Jet engines of fighter aircraft are equipped with fans and compressors. The vibrations of the blades of fans and compressor blades are controlled by midspan dampers. The dampers in the process are subjected to wear and tear. HVOF-sprayed WC–Co coatings are deposited on dampers to improve the life [84]. HVOF

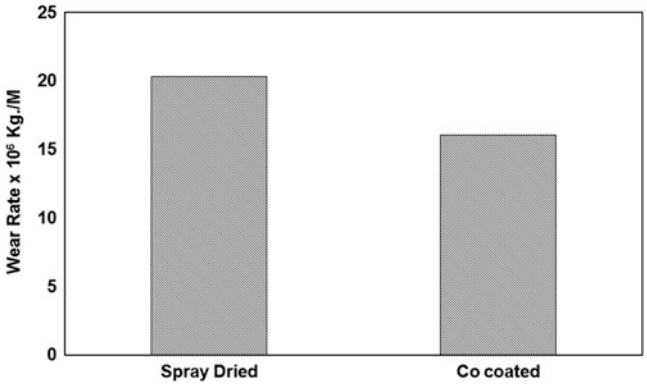

Fig. 1.38 Improvements in abrasive wear resistance of HVOF-sprayed coating obtained by Co-coated porous spray-dried WC–Co nanocomposite powder [83]

Fig. 1.39 WC–Co coating the internal coating of stage III disc of in aircraft engine

WCCoCr used on landing gear for fighter aircraft in US Navy. Also this coating is used on offshore gate valves [85].

Thermal-sprayed WC–Co coating is extensively used in several places of steel industry. Continuous casting moulds are coated with WC–Co coating. The top of the mould is coated with thin WC–Co coating which can withstand high thermal stress in the zone of the molten steel meniscus. At the bottom, thick coating which can withstand high ferrostatic pressure and thereby prevent cracking and spalling of the coating [86] are used.

Briddle rolls are used to control the tension of steel strips as it passes through the continuous pickling, annealing and galvanising lines. These rolls are conventionally coated with Cr plating and are increasingly replaced by HVOF-sprayed WC–Co coatings due to their superior wear resistance [87]. Similar result is obtained from detonation-sprayed WC–Co coating against Cr plated deflector roll [88].

Fig. 1.40 Thermal-sprayed (**a**) WC–Co-coated mixer impeller and (**b**) electric arc-sprayed stainless steel coated in tapered centre portion of forged lifting lid

WC-(10–15)% Co thermal-sprayed coatings are applied to galvanising hardware due to their superior liquid metal erosion resistance relative to Fe and cobalt alloy [89–91]. However, success of this coating under such circumstance depends on reaction between WC and Co phases to improve the poor corrosion properties of Co in molten Zn.

Murakawa and Watanabe [92] demonstrated that an ironing die when coated with plasma-sprayed WC–Co coatings followed by vacuum sintering and hipping, not only resulted improved life of the die and increased output but also resulted in an improved surface finish of the product. Picas et al. [93] demonstrated that thermal-sprayed CrC–NiCr is a very good substitute for hard chromium plating for pistons and valves of automotive engines.

Oxide ceramics offer the benefit of a high melting point, high hardness and wear resistance and chemical stability at high temperature in molten metal environments [94, 95]. Many oxides, particularly Al_2O_3 and yttria-stabilized zirconia are not wetted by liquid zinc and are therefore particularly resistant to corrosion. Such properties make oxide-based coatings particularly attractive for high temperature, high Al-content, and galvalume baths where the more common WC–Co-based coatings do not perform well [96] against liquid metal erosion.

As the solidifying steel exits the mould, it is supported by a series of retaining rolls which redirect it from a vertical orientation to a horizontal run-out bed and cutting operations. These rolls are subjected to high temperatures (steady state of 500–600 °C) and thermal cycling [97] resulting from unavoidable stoppages during casting operations [97]. Large stresses are generated in the rolls from the ferrostatic pressure head of molten steel within the solidified steel shell and the weight of the steel strand itself [97]. To accommodate this, all four faces are supported by closely spaced rolls at the exit of the mould, while only two faces are supported further along the casting line. Cooling water sprays introduce corrosion issues from steam

oxidation and contribute to issues of thermal cracking [97]. Abrasive wear of the roll surfaces results from steel oxides, casting slag and mineral deposits which reduce the roll diameters below acceptable limits [97]. In assessing the performance of detonation-sprayed Cr_3C_2–25NiCr coatings, Wang et al. [98, 99] noted the formation of 'alligator cracks' on the surface of uncoated rolls after 3,740 heats, while coated rolls showed no changes after 12,000 heats [99]. Sanz [97] trailed several chemically hardened TS coatings (HVOF WC–17 % Co coated with a dense chemically blended Cr_2O_3 + SiO_2 + Al_2O_3 based oxide layer) which showed superior wear resistance and lower abrasion rates relative to a new generation weld overlay coating (weld composition: Fe, Nb 0.637, Ni 13.78, Mo 1.39, Cr 17.43, Mn 3.58, Si 0.67 and C 0.062) [98].

1.8 Direction of Future Research

Ever increasing demand for technology has resulted in development of new technique, new materials and new architecture for thermal-sprayed coatings. New era should see development of super hard thermal-sprayed coating. Considerable effort will be diverted for further development of composite and functionally graded thermal-sprayed coatings. Development of smart thermal-sprayed coatings which respond in a selective way to external factors such as stress, temperature, etc. and innovations of new processes such as warm spraying, hybrid thermal spraying, plasma-assisted thermal spraying will draw lot of attention in the years to come.

One important recent development in thermal spraying is cold spray process. Cold spray process can best be used by using expensive helium gases. Improvement in the recovery process made this process quite competitive. Further development in nozzle design, powder quality and process optimisation will result in improved coating performances. To date only limited number of feed stock materials is available for cold spraying. This needs to be upgraded.

Another important development for thermal spraying is nearnet shape components. Substantial research is expected to be directed in the development of removable mandrel and development of complex shape. A larger variety of coatings for near net shape tribology-related components and their increased usage is expected to come in near future.

Over the last decades, various sensors relevant for thermal spraying process and capable of operating under harsh environment of spray booth are developed [100]. Today sensors are available to measure trajectories, temperatures, velocities, sizes and shapes of in-flight particles [101–106]. Infrared cameras and pyrometers are employed to understand the temperature profile of substrate and coatings during preheating, spray process and cooling down [107–115]. Sensors are also developed to measure the stresses within the coatings and evolution of thickness of the coating during spraying [116]. Further development towards improved precision on measurement is expected. New techniques such as shadowgraphs and laser allow precise measurement of particle diameter, which was not hitherto possible.

Development of sensors will allow online control of thermal spraying and thus enhance coating quality and reliability.

There should be more comprehensive database on tribological properties of a larger variety of compositions of cermet coatings. Further effort should be directed for generating data on high temperature wear resistance of cermet coatings and wear behaviour of the said coatings in presence of corrosive fluid.

References

1. Tucker RC Jr (1994) Thermal spray coatings. In: Surface engineering, vol 5, ASM handbook. ASM, Materials Park, OH, p 497
2. Kharlamov YA (1987) Mater Sci Eng 93A:1
3. Fauchais P, Vardelle A, Dussoubs B (2001) J Therm Spray Technol 10:44
4. Pawlowski L (1995) The science and engineering of thermal spray coatings. Wiley, Chichester
5. Wood RJK (2010) Int J Refract Met Hard Mater 28:82
6. Roy M, Pauschitz A, Franek F (2002) In: Proceedings of the 15th international corrosion congress, Grenada, Spain, 22–27 Sept 2002
7. Roy M, Narkhede BE, Paul SN (1999) In: Prashad H (ed) Tribology in 2000 and beyond. Kalajyothi, Hyderabad, India, p 205
8. Kear BH, Sadangi RK, Jain M, Yao R, Kalman Z, Skandan G, Mayo WE (2000) J Therm Spray Technol 9:399
9. Roy M, Pauschitz A, Benardi J, Franek F (2006) J Therm Spray Technol 15(3):372
10. He J, Lavernia EJ (2000) Metall Mater Trans 31A:555
11. Guilemany JM, Calero JA (1997) In: Berndt CC (ed) A united forum for scientific and technological advances. ASM, Materials Park, OH, p 15
12. Roy M, Sundararajan G (1971) In: Proceedings of the 12th international colloquim of tribology, Stuttgart/Ostfilderm, Germany, Jan 2000
13. Mohanty M, Smith RW, De Bonte M, Celis JP, Lugscheider E (1996) Wear 198:251
14. Marshall BD, Noma T, Evans AG (1982) J Am Ceram Soc 65(10):C175
15. Leigh SH, Lin CK, Berndt CC (1995) J Am Ceram Soc 80(8):2093
16. Walpole RE, Myers RH (1978) Probability and statistics for engineers and scientists, 2nd edn. Macmillan, New York
17. Lin CK, Berndt CC (1995) J Mater Sci 30:111
18. Antis GR, Chantikul P, Lawn BR, Marshall DB (1981) J Am Ceram Soc 64:533
19. Evans AG, Charles EA (1976) J Am Ceram Soc 59:371
20. Niihara K, Morena R, Hassleman DPH (1983) In: Bradt RC, Evans AG, Hassleman DP, Lange FF (eds) Fracture mechanics of ceramics. Plenum, New York, p 97
21. Niihara K, Morena R, Hassleman DPH (1982) J Mater Sci Lett 1:13
22. Roy M, Pauschitz A, Franek F (2006) Tribol Int 39:29
23. Greenwood JA, Williamson JBP (1966) Proc R Soc Lond A 295:300
24. Lim SC, Ashby MF (1987) Acta Metall 35:11
25. Zhao XQ, Zhou HD, Chen JM (2006) Mater Sci Eng A431:290
26. Roy M, Pauschitz A, Franek F (2004) Wear 257:799–811
27. Zhu YC, Ding CX (1999) Nanostruct Mater 11:319
28. Rodrıguez J, Martın A, Fernandez R, Fernández JE (2003) Wear 255:950
29. Roy M (2009) Trans Indian Inst Met 62:197
30. Lenling WJ, Smith MF, Henfling JA (1990) In: Proceedings of the third thermal spray conference, Long Beach, CA, p 227

31. Ito H, Nakamura R, Shiroyama M, Sasaki T (1990) In: Proceedings of the third thermal spray conference, Long Beach, CA, p 223
32. Stewart A, Shipway P, Maccartney DG (1998) Surf Coat Technol 105:13
33. Khameneh Asl S, Hyderzadeh Sohi M, Hadavi SMM (2004) Mater Sci Forum 465–466:427
34. Khameneh Asl S, Hyderzadeh Sohi M, Hokamoto K, Umera M (2006) Wear 260:1203
35. Guilemany JM, Miguel JM, Vizcaino S, Lorenzana C, Delgado J, Sanchez J (2002) Surf Coat Technol 157:207
36. Stoica V, Ahmed R, Itsukaichi T (2005) Surf Coat Technol 199:7
37. Stoica V, Ahmed R, Itsukaichib T, Tobe S (2004) Wear 257:1103
38. Stoica V, Ahmed R, Golshan M, Tobe S (2004) J Therm Spray Technol 13:93
39. Mateos J, Cuetos JM, Vijande R, Farnandez E (2001) Tribol Int 34:345
40. Bolelli G, Rauch J, Cannillo V, Killinger A, Lusvarghi L, Gadow R (2009) J Therm Spray Technol 18:35
41. Sudaprasert T, Shipway PH, MaCartney DG (2003) Wear 255:7
42. Maiti AK, Mukhopadhyah N, Raman R (2007) Surf Coat Technol 201:7781
43. Berget J, Rohne T, Bardal E (2007) Surf Coat Technol 201:7619
44. Chivavibul P, Watanabe M, Kuroda S, Shinoda K (2007) Surf Coat Technol 202:509
45. Lee CW, Han JH, Yoon J, Shin MC, Kwun SI (2010) Surf Coat Technol 204:2223
46. Karimi A, Verdon C, Barbezat G (1993) Surf Coat Technol 57:81
47. Ozdemir I, Tekmen C, Tsunekawa Y, Grund T (2010) J Therm Spray Technol 19:384
48. Hawthorne HM, Arsenault B, Immarigeon JP, Legoux JG, Parameswaran VR (1999) Wear 225–229:825
49. Levy AV, Wang B (1988) Wear 121:325
50. Barbezat B, Nicoll AR, Sicknger A (1993) Wear 162–164:529
51. Wood RJK, Mellor BG, Binfield ML (1997) Wear 211:70
52. Kim HJ, Kweon YG, Chang RW (1994) J Therm Spray Technol 3:169
53. Roy M, Narkhede BE, Paul SN (1999) In: Proceedings of the 2nd international conference on industrial tribology, Hyderabad, India, 1–4 Dec 1999, p 205
54. Hearley JA, Little JA, Sturgeon AJ (1999) Wear 233–235:328
55. Wang BQ, Verstak A (1999) Wear 233–235:342
56. Smith RW, Mohanty M, Stessel E, Verstak A, Ohmori A (eds) (1995) Thermal spraying-current status and future trends. In: Proceedings of ITSC'95, High Temperature Society of Japan, Osaka, Japan, p 1121
57. Verstak A, Vitiaz P, Lugscheider E (1996) DVS Berichte 175:71, German Welding Society
58. Tayor ML, Murphy JG, King HW (1997) In: Proceedings of ASM symposium on tribological mechanism and wear problems in materials, ASM International, Materials Park, OH, p 143
59. Li CJ, Yang GJ, Ohmori A (2006) Wear 260:1166
60. Tsai PC, Lee JH, Chang C-L (2007) Surf Coat Technol 202:719
61. Kulu P, Hussainova I, Veinthal R (2005) Wear 258:488
62. Uusitalo MA, Vuoristo PMJ, Mäntyla TA (2002) Wear 252:586
63. Wang BQ, Lee SW (1997) Wear 203–204:580
64. Guilemany JM, Cinca N, Fernández J, Sampath S (2008) J Therm Spray Technol 17:762
65. Dent AH, DePalo S, Sampath S (2002) J Therm Spray Technol 11:551
66. Abdel-Samad AA, El-Bahloul AAM, Lugscheider E, Rassoul SA (2000) J Mater Sci 35:3127
67. Gawne DT, Qui Z, Zhang T, Bao Y, Zhang K (2001) J Therm Spray Technol 10:599
68. Liu Y, Fischer T, Dent A (2003) Surf Coat Technol 167:68
69. Habib KA, Saura JJ, Ferrer C, Damra MS, Gimenez E, Cabedo L (2006) Surf Coat Technol 201:1436
70. Nerz JE, Kushner BA, Jr, Rotolico AJ (1991) In: Proceedings of 4th national thermal spraying conference, Pittsburg, PA, 4–10 May 1991
71. Lee HC, Gurland J (1978) Mater Sci Eng 33:125
72. Kumari K, Anand K, Bellaci M, Giannozzi M (2010) Wear 268:1309
73. Stewart DA, Shipway PH, McCartney DG (1998) Surf Coat Technol 105:13

74. Wang Q, Chen ZH, Ding ZX (2009) Tribol Int 42:1046
75. Wirojanupatump S, Shipway PH, McCartney DG (2001) Wear 249:829
76. Zum Ghar KH, Eldis GT (1980) Wear 64:175
77. Thakare MR, Wharton JA, Wood RJK, Menger C (2008) Tribol Int 41:629
78. Stewart DA, Shipway PH, McCartney DG (1999) Wear 225–229:789
79. Qi X, Eigen N, Aust E, Gartner F, Klassen T, Bormann R (2006) Surf Coat Technol 200:5037
80. Kim JH, Baik KH, Seong BG, Hwang SY (2007) Mater Sci Eng A449–551:876
81. Jordan EH, Gell M, Sohn YH, Goberman D, Shaw L, Jiang S, Wang M, Xiao TD, Wang Y, Strutt P (2001) Mater Sci Eng A301:80
82. Gell M, Jordan EH, Sohn YH, Goberman D, Shaw L, Xiao TD (2001) Surf Coat Technol 146–147:48
83. Baik KH, Kim JH, Seong BG (2007) Mater Sci Eng A449–551:846
84. McGrann RTR, Shanley JR (1997) In: Berndt CC (ed) Thermal spray: a united forum for scientific and technological advances. ASM International, Materials Park, OH, p 341
85. Wheeler DW, Wood RJK (2005) Wear 258:526
86. Lavin P (1998) Coating of continuous casting machine components. International Patent, Publication Number WO 98/21379. Monitor Coating and Engineering Limited
87. Sato Y, Midorikawa S, Iwashita Y, Yokogawa A, Takano T (1993) Service life extension technique for cold rolling rolls. Kawasaki Steel Technical Report No. 29, p 74
88. Kasai S, Sato Y, Yanagisawa A, Ichihara A, Onishi H (1987) Development of surface treatment techniques for process rolls in steelworks. Report No. 17, p 81
89. Ren X, Mei X, She J, Ma J (2007) Materials resistance to liquid zinc corrosion of surface of sink roll. In: Proceedings of Sino-Swedish structural materials symposium 2007, p 125
90. Sawa M, Oohori J (1995) In: Ohmri A (ed) Thermal spraying: current status and future tends. Proceedings of 14th international thermal spray conference, Kobe, Japan, 22–26 May 1995. High Temperature Society of Japan, p 37
91. Seong BG, Hwang SY, Kim MC, Kimin KY (2000) In: Berndt CC (ed) Thermal spray: surface engineering via applied research. Proceedings of 1st international thermal spray conference, Montreal QC, 8–11 May 2000. ASM International, Materials Park, OH, p 1159
92. Murakawa M, Watanabe S (1989) In: Proceedings of 2nd international conference on hot isostatic processing, theory and applications, Gaitherburg, MD, 7–9 June 1989
93. Picas JA, Forn A, Matthaus G (2006) Wear 261:477
94. Dong Y, Yan D, He J, Zhang J, Li X (2006) Surf Coat Technol 201:2455
95. Hollis K, Peters M, Bartram B (2003) In: Moreau C, Marple B (eds) Thermal spray 2003: advancing the science and applying the technology. Proceedings of the 2003 international thermal spray conference, Orlando, FL, 5–8 May 2003. ASM International, Materials Park, OH, p 153
96. Fukubayashi HH (2004) In: Proceedings of the international thermal spray conference 2004, Osaka, 10–12 May 2004. ASM International, Materials Park, OH, p 125
97. Sanz A (2004) Surf Coat Technol 177–178:1
98. Wang J, Zhang L, Sun B, Zhou Y (2000) Surf Coat Technol 130:69
99. Wang J, Sun B, Guo Q, Nishio M, Ogawa H (2002) J Therm Spray Technol 11(2):261
100. Fauchais P, Verdelle M (2010) J Therm Spray Technol 19:668
101. Fauchais P (1992) J Therm Spray Technol 1:117
102. Li CJ, Wu T, Li C-X, Sun B (2003) J Therm Spray Technol 12:80
103. Marple BR, Voyer J, Bisson JF, Moreau C (2001) J Mater Process Technol 117:418
104. Landes K (2006) Surf Coat Technol 201:1948
105. Gougeon P, Moreau C (1993) J Therm Spray Technol 2:229
106. Planche MP, Liao H, Coddet C (2004) Surf Coat Technol 182:215
107. Verdelle M, Renault T, Fauchais P (2002) High Temp Mater Process 6:469
108. Doubenskaia M, Bertrand P, Smurov I (2006) Surf Coat Technol 201:1955
109. Xiaa W, Zangb H, Wanga G, Wanga Y (2009) J Mater Process Technol 209:1955

110. Salimijazi HR, Pershin L, Coyle TW, Mostaghimi J, Chandra S, Lau YC, Rosenzweig L, Moran E (2007) J Therm Spray Technol 16:580
111. Kuroda S, Fukushima T, Kitahara S (1988) Thin Solid Films 164:157
112. Kuroda S, Clyne TW (1991) Thin Solid Films 200:49
113. Clyne TW, Gill SC (1996) J Therm Spray Technol 5:401
114. Matejicek J, Sampath S (2003) Acta Mater 51:863
115. Matejicek J, Sampath S, Gilmore D, Neiser R (2003) Acta Mater 51:873
116. Nadeau A, Pouliot L, Nadeau F, Blain J, Berube SA, Moreau C, Lamontagne M (2006) J Therm Spray Technol 15:744